JCTC Journal of Chemical Theory and Computation

Article

pubs.acs.org/JCTC

Analytical First-Order Molecular Properties and Forces within the Adiabatic Connection Random Phase Approximation

Asbjörn M. Burow,[†] Jefferson E. Bates,[†] Filipp Furche,*[,†] and Henk Eshuis[‡]

[†]University of California, Irvine, Department of Chemistry, 1102 Natural Sciences II, Irvine, California 92697-2025, United States of America

[‡]Montclair State University, Department of Chemistry and Biochemistry, 1 Normal Avenue, Montclair, New Jersey 07043, United States of America

Supporting Information

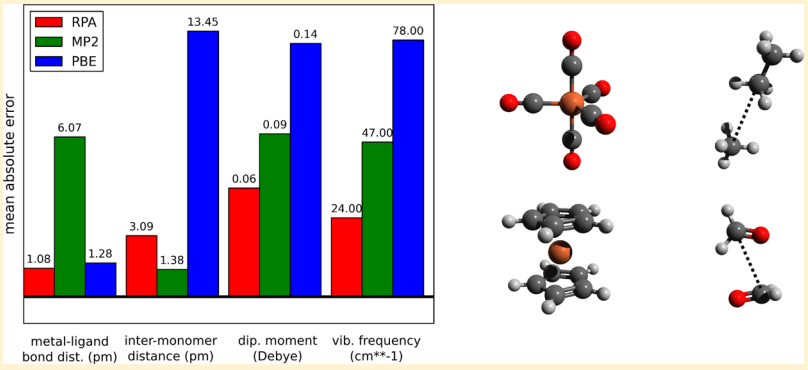

ABSTRACT: The random phase approximation (RPA) is an increasingly popular method for computing molecular ground-state correlation energies within the adiabatic connection fluctuation−dissipation theorem framework of density functional theory. We present an efficient analytical implementation of first-order RPA molecular properties and nuclear forces using the resolution-of-the-identity (RI) approximation and imaginary frequency integration. The centerpiece of our approach is a variational RPA energy Lagrangian invariant under unitary transformations of occupied and virtual reference orbitals, respectively. Its construction requires the solution of a single coupled-perturbed Kohn−Sham equation independent of the number of perturbations. Energy gradients with respect to nuclear displacements and other first-order properties such as one-particle densities or dipole moments are obtained from partial derivatives of the Lagrangian. Our RPA energy gradient implementation exhibits the same $O(N^4 \log N)$ scaling with system size N as a single-point RPA energy calculation. In typical applications, the cost for computing the entire gradient vector with respect to nuclear displacements is ∼5 times that of a single-point RPA energy calculation. Derivatives of the quadrature nodes and weights used for frequency integration are essential for RPA gradients with an accuracy consistent with RPA energies and can be included in our approach. The quality of RPA equilibrium structures is assessed by comparison to accurate theoretical and experimental data for covalent main group compounds, weakly bonded dimers, and transition metal complexes. RPA outperforms semilocal functionals as well as second-order Møller−Plesset (MP2) theory, which fails badly for the transition metal compounds. Dipole moments of polarizable molecules and weakly bound dimers show a similar trend. RPA harmonic vibrational frequencies are nearly of coupled cluster singles, doubles, and perturbative triples quality for a set of main group compounds. Compared to the ring-coupled cluster based implementation of Rekkedal et al. [*J. Chem. Phys.* **2013**, *139*, 081101.], our method scales better by two powers of N and supports a semilocal Kohn−Sham reference. The latter is essential for the good performance of RPA in small-gap systems.

1. INTRODUCTION

A small energy gap between the highest occupied molecular orbital (HOMO) and the lowest unoccupied molecular orbital (LUMO) is characteristic of many d- and f-element compounds and (highly reactive) catalytically active species,[1,2] and their experimental analysis is challenging, giving electronic structure calculations special importance for the study of these systems.[3−5] The bulk of calculations on small-gap compounds nowadays relies on density functional theory (DFT) using semilocal functionals.[6] While popular semilocal functionals such as B3-LYP[7,8] and PBE[9] can be accurate for large-gap main group chemistry, they are generally much less accurate for small gap systems such as many organometallic compounds and transition metal oxides.[10] Moreover, these functionals fail in situations where mid- and long-range noncovalent interactions are important,[11−14] such as the Grubbs' II catalyst.[15,16] Empirical dispersion corrections[17] remedy this problem to some extent

Received: September 29, 2013
Published: November 18, 2013

but are suspect for reactions involving different oxidation states. Some semilocal functionals such as the Minnesota family[18,19] contain a large number of fitted parameters and require careful validation before they can be applied to novel compounds.

Until recently, the validation of semilocal DFT results for small-gap systems using higher-level methods was difficult or impossible. Post-Hartree−Fock (HF) perturbation theory, such as the second-order Møller−Plesset perturbation theory (MP2),[20] fails for small HOMO−LUMO gaps. Single-reference coupled cluster singles, doubles, with perturbative triples [CCSD(T)][21,22] is more stable but hardly affordable even for moderate system sizes of 30 to 100 atoms. Multireference methods such as complete active space self-consistent field with second-order perturbation theory (CASPT2)[23,24] and multireference configuration interaction (MR-CI)[25,26] can provide highly accurate benchmark results but are presently limited to 10−20 correlated electrons.

For small-gap systems, electron correlation methods based on the random phase approximation (RPA) are a promising alternative to low-order perturbative methods and could lead the way out of this dilemma. RPA is nonperturbative and can be applied to a wide range of small- and large-gap situations; it works for molecules,[27−32] surfaces,[33,34] and solids;[35−41] it captures dispersion interactions and achieves reasonable accuracy for covalent bond energies;[32,37,42] it is comparable to MP2 in computational complexity; and it is free of empiricism.

Rekkedal et al. recently reported an implementation of analytical RPA gradients using the HF determinant as a reference.[43] Their method is based on the ring approximation to coupled cluster doubles (CCD) theory[44] and scales as $O(N^6)$ with the system size N. For structures of small main group compounds and rare-gas dimers, Rekkedal et al. found no improvement of RPA over MP2. If this were the final word, RPA structure optimizations would be pointless, since they would not offer better accuracy than the $O(N^5)$ scaling MP2 method.

Our present approach to analytical RPA gradients differs from the one of Rekkedal et al. in two crucial aspects: First, we achieve an $O(N^4 \log N)$ scaling of the operation count and $O(N^3)$ scaling of mass storage by combining resolution-of-the-identity (RI) methods with complex frequency integration.[45] This method entirely avoids the computation of four-index objects such as doubles amplitudes. Second, our implementation is based on a semilocal Kohn−Sham (KS) rather than the HF reference determinant. This is essential for applications to small-gap systems, where RPA has its greatest advantage over MP2. Moreover, the direct or bare RPA is on a much sounder theoretical foundation in a post-KS than in a post-HF framework.[32]

We review the RI-RPA energy functional in section 2.1. An energy Lagrangian, which is stationary with respect to the KS molecular orbitals (MOs) and invariant under unitary transformations of the occupied and virtual KS MOs, respectively, is constructed in section 2.2. This Lagrangian contains additional Lagrange multipliers obtained by solving a *single* coupled-perturbed KS (CPKS) equation, which is independent of the perturbation (section 2.3). This greatly simplifies the derivation of first-order analytical derivatives (section 2.4). The resulting algorithm for first-order property calculations is summarized in section 2.5. Results for equilibrium structures of small main group compounds, transition metal complexes, and weakly bound complexes are compared to other methods and experimental data in section 3. We also assess the quality of RPA dipole moments and vibrational frequencies for small main group compounds. Conclusions for computational practice and method development are drawn in section 4. Table 1 lists symbols used throughout this work.

2. THEORY

2.1. Review of the RI-RPA Energy Functional. Present-day RPA calculations are "post-KS"; that is, they require a KS reference determinant $|\Phi\rangle$ as input. Thus, the first step of a RPA calculation involves solution of the KS equations,

$$\mathbf{F}_\sigma \mathbf{C}_\sigma = \mathbf{S}\mathbf{C}_\sigma \boldsymbol{\varepsilon}_\sigma \tag{1}$$

to determine the KS MO coefficients $C_{\mu p\sigma}$. In the following, Greek indices denote atomic orbital (AO) basis functions, $\sigma = \alpha, \beta$ is a spin index, and lower case Roman indices $i, j, \ldots$ label occupied, $a, b, \ldots$ virtual, and $p, q, \ldots$ general KS MOs. We assume real MOs and consider a spin-unrestricted reference throughout this paper; supervectors $\mathbf{C} = (\mathbf{C}_\alpha, \mathbf{C}_\beta)$ and $\boldsymbol{\varepsilon} = (\boldsymbol{\varepsilon}_\alpha, \boldsymbol{\varepsilon}_\beta)$ are used wherever it is convenient; further simplifications apply in the spin-restricted case. The one-particle effective KS Hamiltonian,

$$F_{\mu\nu\sigma} = h_{\mu\nu\sigma} + \sum_{\kappa\lambda\sigma'} (\mu\nu|\kappa\lambda) D_{\kappa\lambda\sigma'} + V^{\mathrm{XC}}_{\mu\nu\sigma}[\mathbf{D}] \tag{2}$$

contains the one-electron Hamiltonian $\mathbf{h}$, the matrix of the electrostatic Coulomb or Hartree potential, and the exchange-correlation (XC) potential matrix $\mathbf{V}^{\mathrm{XC}}$. For generality, $\mathbf{h}$ is assumed to be spin-dependent throughout this paper. $(\mu\nu|\kappa\lambda)$ is an electron repulsion integral (ERI) in Mulliken notation,

$$(\mu\nu|\kappa\lambda) = \int d^3r_1 \int d^3r_2 \frac{\chi_\mu(\mathbf{r}_1)\chi_\nu(\mathbf{r}_1)\chi_\kappa(\mathbf{r}_2)\chi_\lambda(\mathbf{r}_2)}{|\mathbf{r}_1 - \mathbf{r}_2|} \tag{3}$$

the $\{\chi_\mu\}$ stands for atom-centered Gaussian basis functions. The KS spin-unrestricted density matrix,

$$D_{\mu\nu\sigma} = \sum_i C_{\mu i\sigma} C_{\nu i\sigma} \tag{4}$$

depends on the MO coefficients, making eigenvalue problem 1 nonlinear. Within the Handy−Neumann approximation,[46] the XC potential matrix is given by[47]

$$V^{\mathrm{XC}}_{\mu\nu\sigma} = \frac{\partial E^{\mathrm{XC}}}{\partial D_{\mu\nu\sigma}} \tag{5}$$

where E^{XC} is a semilocal approximation to the XC energy functional. At the self-consistent solution of eq 1, the occupied−virtual blocks of the Lagrange multiplier matrix $\boldsymbol{\varepsilon}$ vanish. To preserve invariance of the formalism under transformation of occupied and virtual MOs, respectively, and to avoid instabilities due to orbital degeneracies in the canonical formalism,[48,49] we will not assume that $\boldsymbol{\varepsilon}$ is diagonal. The MO coefficients are required to be $\mathbf{S}$-orthonormal,

$$\mathbf{C}_\sigma^{\mathrm{T}} \mathbf{S} \mathbf{C}_\sigma = \mathbf{1} \tag{6}$$

where $\mathbf{S}$ is the overlap matrix of the nonorthogonal AO basis $\{\chi_\mu\}$. This implies orthonormality of the MOs

$$\phi_{p\sigma}(\mathbf{r}) = \sum_\mu C_{\mu p\sigma} \chi_\mu(\mathbf{r}) \tag{7}$$

Once the KS reference determinant has been computed, the RI-RPA total energy is obtained as

Table 1. Symbols Used Throughout This Work and Number of Spin Components ($N_s = 2$), all MOs (N_{MO}), Occupied MOs (N_{occ}), Virtual MOs (N_{virt}), Occupied Times Virtual MOs (N_{ov}), AO Basis Functions (N_{AO}), and Auxiliary Basis Functions (N_{aux}) Are Used to Define Matrix Dimensions[a]

scalar	name	eq
$\hat{H}$	full electronic Hamiltonian	
$\|\Phi\rangle$	KS reference determinant	
$E^{\langle\text{superscript}\rangle}$	energy of the corresponding superscript	8
L^{RIRPA}	Lagrangian	21
$\phi_{p\sigma}$	molecular orbital	7
χ_μ	Gaussian AO basis function	
η_P	Gaussian auxiliary basis function	
ω	frequency	
ξ	perturbation	

(super) matrix	name	eq	dimensions
$\boldsymbol{\varepsilon}$	MO KS matrix	1	$N_s \times N_{MO} \times N_{MO}$
$\mathbf{F}$	AO KS matrix	2	$N_s \times N_{AO} \times N_{AO}$
$\boldsymbol{\varepsilon}^{\text{HF}}$	MO HF matrix at the KS reference	37	$N_s \times N_{MO} \times N_{MO}$
$\mathbf{F}^{\text{HF}}$	AO HF matrix at the KS reference	38	$N_s \times N_{AO} \times N_{AO}$
$\mathbf{h}$	AO one-electron Hamiltonian matrix		$N_s \times N_{AO} \times N_{AO}$
$\mathbf{V}^{\text{XC}}$	AO exchange-correlation potential matrix	5	$N_s \times N_{AO} \times N_{AO}$
$\mathbf{S}$	AO overlap matrix		$N_{AO} \times N_{AO}$
$\mathbf{C}$	MO coefficients		$N_s \times N_{AO} \times N_{MO}$
$\mathbf{D}^{\text{RIRPA}}$	AO rel. RI-RPA ODM	46	$N_s \times N_{AO} \times N_{AO}$
$\mathbf{D}$	AO KS ODM	4	$N_s \times N_{AO} \times N_{AO}$
$\mathbf{D}^{\Delta}$	MO rel. RI-RPA difference ODM	28	$N_s \times N_{MO} \times N_{MO}$
$\mathbf{D}^{\Delta\text{AO}}$	AO rel. RI-RPA difference ODM	45	$N_s \times N_{AO} \times N_{AO}$
$\mathbf{T}$	MO unrel. ODM due to correlation	29, 58	$N_s \times N_{MO} \times N_{MO}$
$\mathbf{T}^{\text{AO}}$	AO unrel. ODM due to correlation	cf. eq 45	$N_s \times N_{AO} \times N_{AO}$

(super) matrix	name	eq	dimensions
$\mathbf{Q}$	equivalent of a single ring diagram	14	$N_{aux} \times N_{aux}$
$\boldsymbol{\Pi}^{(4)}$	4-center AO ERIs	3	$N_{AO}^2 \times N_{AO}^2$
$\boldsymbol{\Pi}^{(3)}$	3-center AO−auxiliary ERIs	11	$N_{AO}^2 \times N_{aux}$
$\boldsymbol{\Pi}^{(2)}$	2-center auxiliary ERIs	11	$N_{aux} \times N_{aux}$
$\mathbf{X}$	supervector of AO parameters	18	
$\boldsymbol{\Lambda}$	upper triangular Cholesky factor	12	$N_{aux} \times N_{aux}$
$\mathbf{B}$	Cholesky-weighted 3-index ERIs	13	$N_s \times N_{ov} \times N_{aux}$ or $N_s \times N_{MO} \times N_{MO} \times N_{aux}$
$\mathbf{G}$	frequency-dependent supermatrix	15	$N_s \times N_{ov} \times N_s \times N_{ov}$
$\boldsymbol{\Delta}$	noninteracting excitation energies	16	$N_s \times N_{ov} \times N_s \times N_{ov}$
$\tilde{\mathbf{Q}}$	function of $\mathbf{Q}$	32	$N_{aux} \times N_{aux}$
$\mathbf{R}$	right-hand side of CPKS equation	36	$N_s \times N_{ov}$
$\boldsymbol{\gamma}$	2-index matrix from RI-RPA MO derivatives	39, 64	$N_s \times N_{MO} \times N_s \times N_{MO}$
$\mathbf{Z}$	MO relaxation-only RI-RPA ODM	33	$N_s \times N_{MO} \times N_{MO}$
$\mathbf{W}$	MO rel. energy-weighted ODM	41	$N_s \times N_{MO} \times N_{MO}$
$\mathbf{W}^{\text{AO}}$	AO rel. energy-weighted ODM	cf. 45	$N_s \times N_{AO} \times N_{AO}$
$\mathbf{H}^+$	supermatrix for the CPKS equation	34	$N_s \times N_{MO}^2 \times N_s \times N_{MO}^2$
$\boldsymbol{\Gamma}^{(4)}$	AO 4-index rel. TDM	50	$N_{AO}^2 \times N_{AO}^2$
$\boldsymbol{\Gamma}^{(3)}$	AO-auxiliary 3-index rel. TDM	51	$N_{aux} \times N_{AO}^2$
$\boldsymbol{\Gamma}^{(2)}$	auxiliary 2-index rel. TDM	52	$N_{aux} \times N_{aux}$

[a]Abbreviations: ODM and TDM = one- and two-particle density matrix, ERI = electron repulsion integral, rel. = relaxed, and unrel. = unrelaxed.

$$E^{\text{RIRPA}} = \langle\Phi|\hat{H}|\Phi\rangle + E^{\text{C RIRPA}} \tag{8}$$

$\hat{H}$ is the full electronic Hamiltonian, and the expectation value

$$\langle\Phi|\hat{H}|\Phi\rangle = \sum_{\mu\nu\sigma} D_{\mu\nu\sigma} h_{\mu\nu\sigma} + \frac{1}{2}\sum_{\mu\nu\sigma}\sum_{\kappa\lambda\sigma'} (\mu\nu|\kappa\lambda) \times [D_{\mu\nu\sigma}D_{\kappa\lambda\sigma'} - \delta_{\sigma\sigma'}D_{\mu\kappa\sigma}D_{\nu\lambda\sigma'}] \tag{9}$$

equals the HF energy functional evaluated at the KS MO coefficients $\mathbf{C}$. The RI-RPA correlation energy is efficiently computed as an integral over imaginary frequency ω,[45]

$$E^{\text{C RIRPA}} = \frac{1}{2}\int_{-\infty}^{\infty}\frac{d\omega}{2\pi}\langle\ln(\mathbf{1}_{aux} + \mathbf{Q}(\omega)) - \mathbf{Q}(\omega)\rangle \tag{10}$$

where brackets denote the trace operation. Matrix $\mathbf{Q}(\omega)$ is the equivalent of a single ring diagram in the many-body perturbation expansion of the ground state[32] and has the dimension $N_{aux} \times N_{aux}$, where N_{aux} is the number of atom-centered auxiliary basis functions η_P. This auxiliary basis provides an approximate factorization of the ERI supermatrix $\Pi^{(4)}_{\mu\nu\kappa\lambda} = (\mu\nu|\kappa\lambda)$ according to

$$\boldsymbol{\Pi}^{(4)}_{\text{RI}} = \boldsymbol{\Pi}^{(3)}(\boldsymbol{\Pi}^{(2)})^{-1}(\boldsymbol{\Pi}^{(3)})^{\text{T}} \tag{11}$$

where $\Pi^{(3)}_{\mu\nu P} = (\mu\nu|P)$ and $\Pi^{(2)}_{PQ} = (P|Q)$ denote three- and two-center ERIs, respectively. $(\boldsymbol{\Pi}^{(2)})^{-1}$ is computed from the Cholesky decomposition

$$\boldsymbol{\Pi}^{(2)} = \boldsymbol{\Lambda}^{\text{T}}\boldsymbol{\Lambda} \tag{12}$$

where $\boldsymbol{\Lambda}$ is upper triangular. This "Coulomb metric"[50,51] leads to a variational upper bound for the RPA correlation energy.[32] Defining

$$B_{pq\sigma P} = \sum_{\mu\nu Q} C_{\mu p\sigma} C_{\nu q\sigma} (\mu\nu|Q)(\boldsymbol{\Lambda}^{-1})_{QP} \tag{13}$$

$\mathbf{Q}$ is given by

$$\mathbf{Q} = 2\mathbf{B}^{\text{T}}\mathbf{G}\mathbf{B} \tag{14}$$

$\mathbf{G}$ is a frequency-dependent supermatrix,

$$\mathbf{G} = \boldsymbol{\Delta}(\boldsymbol{\Delta}^2 + \omega^2\mathbf{1})^{-1} \tag{15}$$

where

$$\Delta_{ia\sigma jb\sigma'} = \delta_{\sigma\sigma'}(\varepsilon_{ab\sigma}\delta_{ij} - \varepsilon_{ij\sigma}\delta_{ab}) \tag{16}$$

contains the virtual−virtual and occupied−occupied blocks of the Lagrange multiplier matrix $\boldsymbol{\varepsilon}$. The imaginary frequency integral in eq 10 is carried out numerically using exponentially convergent Clenshaw−Curtis quadrature with a geometry-dependent optimized scaling parameter.[52] We neglect the resulting quadrature error in the following. Finite frequency grids lead to additional terms in the first-order RPA properties

dx.doi.org/10.1021/ct4008553 | J. Chem. Theory Comput. 2014, 10, 180−194

due to quadrature weight derivatives and are discussed in Appendix B.

G is related to the matrix representation of the noninteracting KS polarization propagator[53] at imaginary frequencies $i\omega$. The KS density−density response function at imaginary frequencies is

$$\chi_{0\sigma\sigma'}(i\omega, \mathbf{r}, \mathbf{r}') = -2\sum_{iajb} G_{ia\sigma jb\sigma'}(\omega)\phi_{i\sigma}(\mathbf{r})\phi_{a\sigma}(\mathbf{r})\phi_{j\sigma'}(\mathbf{r}')\phi_{b\sigma'}(\mathbf{r}') \tag{17}$$

and matrix $\mathbf{1}_{\text{aux}} + \mathbf{Q}$ may be viewed as an auxiliary basis representation of the dielectric function.[54]

2.2. Lagrangian of the RI-RPA Energy. The RI-RPA energy, eq 8, is a function of the MO coefficients **C** and the Lagrange multipliers $\boldsymbol{\varepsilon}$ and depends parametrically (i) on the interacting Hamiltonian $\hat{H}$, (ii) on the AO basis functions χ_μ and the auxiliary basis functions η_P. All parameters may be gathered in a supervector

$$\mathbf{X} = (\mathbf{h}, \mathbf{\Pi}^{(4)}, \mathbf{\Pi}^{(3)}, \mathbf{\Pi}^{(2)}) \tag{18}$$

and thus

$$E^{\text{RIRPA}} \equiv E^{\text{RIRPA}}(\mathbf{C}, \boldsymbol{\varepsilon}|\mathbf{X}) \tag{19}$$

C and $\boldsymbol{\varepsilon}$ in turn depend parametrically on **X**, $\mathbf{V}^{\text{XC}}$, and **S** through the KS eq 1 and the orthonormality constraint 6. First-order properties may be defined in a rigorous and general fashion as total derivatives of the energy with respect to a "perturbation" parameter ξ;[55] ξ may represent, for example, a Cartesian nuclear displacement or a uniform electric field. Straightforward differentiation of the RI-RPA energy using eq 19 yields

$$\frac{\mathrm{d}E^{\text{RIRPA}}(\mathbf{C}, \boldsymbol{\varepsilon}|\mathbf{X})}{\mathrm{d}\xi} = \left\langle \left(\frac{\partial E^{\text{RIRPA}}}{\partial \mathbf{C}}\right)_{\boldsymbol{\varepsilon},\mathbf{X}} \frac{\mathrm{d}\mathbf{C}}{\mathrm{d}\xi} \right\rangle + \left\langle \left(\frac{\partial E^{\text{RIRPA}}}{\partial \boldsymbol{\varepsilon}}\right)_{\mathbf{C},\mathbf{X}} \frac{\mathrm{d}\boldsymbol{\varepsilon}}{\mathrm{d}\xi} \right\rangle + \left\langle \left(\frac{\partial E^{\text{RIRPA}}}{\partial \mathbf{X}}\right)_{\mathbf{C},\boldsymbol{\varepsilon}} \frac{\mathrm{d}\mathbf{X}}{\mathrm{d}\xi} \right\rangle \tag{20}$$

where we assume that traces are formed separately for each element of **X**.

Fast evaluation of the first-order energy derivatives for all nuclear displacements is crucial for structure optimizations. For Gaussian AO and auxiliary basis sets, $\mathrm{d}\mathbf{X}/\mathrm{d}\xi$ is sparse and may be obtained by analytical differentiation of AO integrals;[56,57] however, $\mathrm{d}\mathbf{C}/\mathrm{d}\xi$ and $\mathrm{d}\boldsymbol{\varepsilon}/\mathrm{d}\xi$ are *not* sparse; their computation for all f nuclear degrees of freedom would require the solution of f CPKS equations, making the calculation of RI-RPA energy gradients an order of magnitude more expensive than single-point energies. It is elementary but tedious to eliminate the derivatives of MO coefficients and Lagrange multipliers from eq 20 using the Sternheimer−Dalgarno interchange theorem.[58,59] Instead, we adopt an approach in the spirit of Helgaker and Jørgensen,[60] which avoids MO coefficient derivatives in the first place: We define the RI-RPA energy Lagrangian

$$L^{\text{RIRPA}}(\mathcal{C}, \mathcal{E}, \mathcal{D}^{\Delta}, \mathcal{W}|\mathbf{X}, \mathbf{V}^{\text{XC}}, \mathbf{S}) = E^{\text{RIRPA}}(\mathcal{C}, \mathcal{E}|\mathbf{X}) + \sum_{\sigma} (\langle \mathcal{D}^{\Delta}_{\sigma}(\mathcal{C}_{\sigma}^{\mathrm{T}}\mathbf{F}_{\sigma}\mathcal{C}_{\sigma} - \mathcal{E}_{\sigma})\rangle - \langle \mathcal{W}_{\sigma}(\mathcal{C}_{\sigma}^{\mathrm{T}}\mathbf{S}\mathcal{C}_{\sigma} - \mathbf{1})\rangle) \tag{21}$$

$\mathcal{C}$, $\mathcal{E}$, $\mathcal{D}^{\Delta}$, and $\mathcal{W}$ are independent variables. As opposed to the RI-RPA energy, which is not stationary at the KS orbitals **C** and Lagrange multipliers $\boldsymbol{\varepsilon}$, L^{RIRPA} is required to be stationary with respect to $\mathcal{C}$, $\mathcal{E}$, $\mathcal{D}^{\Delta}$, and $\mathcal{W}$. $\mathcal{D}^{\Delta}$ and $\mathcal{W}$ act as Lagrange multipliers enforcing that $\mathcal{C}$ and $\mathcal{E}$ satisfy the KS eqs 1 and the orthonormality constraint 6,

$$\left(\frac{\partial L^{\text{RIRPA}}}{\partial \mathcal{D}^{\Delta}_{\sigma}}\right)_{\text{stat}} = \mathcal{C}_{\sigma}^{\mathrm{T}}\mathbf{F}_{\sigma}\mathcal{C}_{\sigma} - \mathcal{E}_{\sigma} = \mathbf{0} \tag{22}$$

$$\left(\frac{\partial L^{\text{RIRPA}}}{\partial \mathcal{W}_{\sigma}}\right)_{\text{stat}} = \mathcal{C}_{\sigma}^{\mathrm{T}}\mathbf{S}\mathcal{C}_{\sigma} - \mathbf{1} = \mathbf{0} \tag{23}$$

$\mathcal{D}^{\Delta}$ and $\mathcal{W}$ are determined by the remaining stationarity conditions,

$$\left(\frac{\partial L^{\text{RIRPA}}}{\partial \mathcal{E}}\right)_{\text{stat}} = \mathbf{0} \tag{24}$$

and

$$\left(\frac{\partial L^{\text{RIRPA}}}{\partial \mathcal{C}}\right)_{\text{stat}} = \mathbf{0} \tag{25}$$

as shown in section 2.3. Thus, at the stationary point "stat = ($\mathcal{C}$ = **C**, $\mathcal{E}$ = $\boldsymbol{\varepsilon}$, $\mathcal{D}^{\Delta}$ = $\mathbf{D}^{\Delta}$, $\mathcal{W}$ = **W**)",

$$E^{\text{RIRPA}}(\mathbf{C}, \boldsymbol{\varepsilon}|\mathbf{X}) = L^{\text{RIRPA}}(\mathcal{C}, \mathcal{E}, \mathcal{D}^{\Delta}, \mathcal{W}|\mathbf{X}, \mathbf{V}^{\text{XC}}, \mathbf{S})|_{\text{stat}} \tag{26}$$

Since the partial derivatives of L^{RIRPA} with respect to $\mathcal{C}$, $\mathcal{E}$, $\mathcal{D}^{\Delta}$, and $\mathcal{W}$ vanish at the stationary point, first-order RI-RPA properties are efficiently obtained from

$$\frac{\mathrm{d}E^{\text{RIRPA}}(\mathbf{C}, \boldsymbol{\varepsilon}|\mathbf{X})}{\mathrm{d}\xi} = \left\langle \left(\frac{\partial L^{\text{RIRPA}}}{\partial \mathbf{X}}\right)_{\text{stat}} \frac{\mathrm{d}\mathbf{X}}{\mathrm{d}\xi} \right\rangle + \left\langle \left(\frac{\partial L^{\text{RIRPA}}}{\partial \mathbf{V}^{\text{XC}}}\right)_{\text{stat}} \left(\frac{\partial \mathbf{V}^{\text{XC}}}{\partial \xi}\right)_{\text{stat}} \right\rangle + \left\langle \left(\frac{\partial L^{\text{RIRPA}}}{\partial \mathbf{S}}\right)_{\text{stat}} \frac{\mathrm{d}\mathbf{S}}{\mathrm{d}\xi} \right\rangle \tag{27}$$

without the need for derivatives of MO coefficients or derivatives of Lagrange multipliers.

2.3. Lagrange Multipliers $\mathbf{D}^{\Delta}$ and W. $\mathbf{D}^{\Delta}$ and **W** represent intrinsic properties of the RPA ground state that do not depend on the type or number of external perturbations. The derivatives in eqs 24 and 25 are worked out in Appendix A and lead to the following result:

$$\mathbf{D}^{\Delta} = \mathbf{T} + \mathbf{Z} \tag{28}$$

with matrix **T** given by

$$T_{ij\sigma} = \int_{-\infty}^{\infty} \frac{\mathrm{d}\omega}{2\pi} \sum_{a} (\tilde{\mathbf{M}}(\omega) - \omega^2 \mathbf{\Delta}^{-1}\tilde{\mathbf{M}}(\omega)\mathbf{\Delta}^{-1})_{ia\sigma ja\sigma} \tag{29}$$

$$T_{ab\sigma} = -\int_{-\infty}^{\infty} \frac{\mathrm{d}\omega}{2\pi} \sum_{i} (\tilde{\mathbf{M}}(\omega) - \omega^2 \mathbf{\Delta}^{-1}\tilde{\mathbf{M}}(\omega)\mathbf{\Delta}^{-1})_{ia\sigma ib\sigma} \tag{30}$$

the occupied−virtual and virtual−occupied blocks of **T** are zero. The symmetric supermatrix

$$\tilde{\mathbf{M}} = \mathbf{G}\mathbf{B}\tilde{\mathbf{Q}}\mathbf{B}^{\mathrm{T}}\mathbf{G} \tag{31}$$

is never explicitly computed. Matrix $\tilde{\mathbf{Q}}$ is of dimension $N_{\text{aux}} \times N_{\text{aux}}$ and a function of **Q** defined in eq 14,

dx.doi.org/10.1021/ct4008553 | J. Chem. Theory Comput. 2014, 10, 180−194

$$\tilde{\mathbf{Q}} = (\mathbf{1}_{\mathrm{aux}} + \mathbf{Q}(\omega))^{-1} - \mathbf{1}_{\mathrm{aux}} \tag{32}$$

$\mathbf{Z}$ is the solution of a single CPKS equation,

$$(\boldsymbol{\Delta} + \mathbf{H}^{+}_{\mathbf{ovov}})\mathbf{Z}_{\mathbf{ov}} = -\frac{1}{2}\mathbf{R} \tag{33}$$

only the occupied−virtual ($\mathbf{Z}_{\mathrm{ov}}$) and virtual−occupied parts of $\mathbf{Z}$ are nonzero. Here, we introduced the occupied−virtual part $\mathbf{H}^{+}_{\mathbf{ovov}}$ of the supermatrix

$$H^{+}_{pq\sigma rs\sigma'} = 2\sum_{\mu\nu\kappa\lambda} C_{\mu p\sigma} C_{\nu q\sigma}[(\mu\nu|\kappa\lambda) + f^{\mathrm{XC}}_{\mu\nu\sigma\kappa\lambda\sigma'}] C_{\kappa r\sigma'} C_{\lambda s\sigma'} \tag{34}$$

where

$$f^{\mathrm{XC}}_{\mu\nu\sigma\kappa\lambda\sigma'} = \frac{\partial^2 E^{\mathrm{XC}}}{\partial D_{\mu\nu\sigma}\partial D_{\kappa\lambda\sigma'}} \tag{35}$$

is a matrix element of the adiabatic XC kernel[61,62] derived from the semilocal XC energy functional used to generate the reference determinant $|\Phi\rangle$ in eq 1. The CPKS right-hand side is

$$R_{ia\sigma} = 2\varepsilon^{\mathrm{HF}}_{ia\sigma} + \gamma_{ia\sigma} - \gamma_{ai\sigma} + (\mathbf{H}^{+}\mathbf{T})_{ia\sigma} \tag{36}$$

where

$$\boldsymbol{\varepsilon}^{\mathrm{HF}}_{\sigma} = \mathbf{C}^{\mathrm{T}}_{\sigma}\mathbf{F}^{\mathrm{HF}}_{\sigma}\mathbf{C}_{\sigma} \tag{37}$$

with

$$F^{\mathrm{HF}}_{\mu\nu\sigma} = h_{\mu\nu\sigma} + \sum_{\kappa\lambda\sigma'}[(\mu\nu|\kappa\lambda) - \delta_{\sigma\sigma'}(\mu\kappa|\nu\lambda)]D_{\kappa\lambda\sigma'} \tag{38}$$

denoting the Fock matrix evaluated at the KS density matrix $\mathbf{D}$. Matrix $\boldsymbol{\gamma}$ is defined by

$$\gamma_{ap\sigma} = 2\int_{-\infty}^{\infty}\frac{\mathrm{d}\omega}{2\pi}\sum_{j}(\mathbf{GB}\tilde{\mathbf{Q}}\mathbf{B}^{\mathrm{T}})_{ja\sigma jp\sigma} \tag{39}$$

$$\gamma_{ip\sigma} = 2\int_{-\infty}^{\infty}\frac{\mathrm{d}\omega}{2\pi}\sum_{b}(\mathbf{GB}\tilde{\mathbf{Q}}\mathbf{B}^{\mathrm{T}})_{ib\sigma pb\sigma} \tag{40}$$

Once $\mathbf{Z}$ has been obtained from the CPKS eq 33, the difference density matrix due to correlation, $\mathbf{D}^{\Delta}$, eq 28, is computed. Finally, the symmetric Lagrange multiplier matrix $\mathbf{W}$ is obtained as

$$\begin{aligned} W_{ij\sigma} &= \frac{1}{2}\gamma_{ij\sigma} + (\mathbf{T}_{\sigma}\boldsymbol{\varepsilon}_{\sigma})_{ij} + \varepsilon^{\mathrm{HF}}_{ij\sigma} + \frac{1}{2}(\mathbf{H}^{+}\mathbf{D}^{\Delta})_{ij\sigma} \\ W_{ab\sigma} &= \frac{1}{2}\gamma_{ab\sigma} + (\mathbf{T}_{\sigma}\boldsymbol{\varepsilon}_{\sigma})_{ab} \\ W_{ai\sigma} &= \frac{1}{2}\gamma_{ai\sigma} + (\mathbf{Z}_{\sigma}\boldsymbol{\varepsilon}_{\sigma})_{ai} \end{aligned} \tag{41}$$

2.4. Analytical First-Order Derivatives. Using the stationarity of the RI-RPA Lagrangian and inserting the definition of $\mathbf{X}$, eq 18, eq 27 may be expanded as follows:

$$\begin{aligned} \frac{\mathrm{d}E^{\mathrm{RIRPA}}(\mathbf{C},\boldsymbol{\varepsilon}|\mathbf{X})}{\mathrm{d}\xi} &= \left\langle \mathbf{D}^{\mathrm{RIRPA}}\frac{\mathrm{d}\mathbf{h}}{\mathrm{d}\xi}\right\rangle + \left\langle \boldsymbol{\Gamma}^{(4)}\frac{\mathrm{d}\boldsymbol{\Pi}^{(4)}}{\mathrm{d}\xi}\right\rangle \\ &+ \left\langle \mathbf{D}^{\Delta\mathrm{AO}}\left(\frac{\partial\mathbf{V}^{\mathrm{XC}}[\mathbf{D}]}{\partial\xi}\right)_{\mathrm{stat}}\right\rangle + \left\langle \boldsymbol{\Gamma}^{(3)}\frac{\mathrm{d}\boldsymbol{\Pi}^{(3)}}{\mathrm{d}\xi}\right\rangle \\ &+ \left\langle \boldsymbol{\Gamma}^{(2)}\frac{\mathrm{d}\boldsymbol{\Pi}^{(2)}}{\mathrm{d}\xi}\right\rangle - \left\langle \mathbf{W}^{\mathrm{AO}}\frac{\mathrm{d}\mathbf{S}}{\mathrm{d}\xi}\right\rangle \end{aligned} \tag{42}$$

The RI-RPA one-particle density matrix $\mathbf{D}^{\mathrm{RIRPA}}$ may now be identified as

$$\mathbf{D}^{\mathrm{RIRPA}} = \left(\frac{\partial L^{\mathrm{RIRPA}}}{\partial\mathbf{h}}\right)_{\mathrm{stat}} = \mathbf{D} + \mathbf{D}^{\Delta\mathrm{AO}} \tag{43}$$

$$= \mathbf{D} + \mathbf{T}^{\mathrm{AO}} + \mathbf{Z}^{\mathrm{AO}} \tag{44}$$

where

$$\mathbf{D}^{\Delta\mathrm{AO}}_{\sigma} = \mathbf{C}_{\sigma}\mathbf{D}^{\Delta}_{\sigma}\mathbf{C}^{\mathrm{T}}_{\sigma} \tag{45}$$

corrects the KS density matrix $\mathbf{D}$ for correlation and orbital relaxation effects. By construction,

$$\mathbf{D}^{\mathrm{RIRPA}} = \frac{\mathrm{d}E^{\mathrm{RIRPA}}(\mathbf{C},\boldsymbol{\varepsilon}|\mathbf{X})}{\mathrm{d}\mathbf{h}} \tag{46}$$

Thus, $\mathbf{D}^{\mathrm{RIRPA}}$ is the total derivative of the RI-RPA ground state energy with respect to the one-electron Hamiltonian. This fundamental definition of the one-particle density matrix[63] does not require a variational wave function, which is not available for RPA and other approximate electronic structure methods. It is instructive to compare $\mathbf{D}^{\mathrm{RIRPA}}$, eq 46, with

$$\mathbf{T}^{\mathrm{AO}} = \frac{\partial E^{\mathrm{C\,RIRPA}}(\mathbf{C},\boldsymbol{\varepsilon}|\mathbf{X})}{\partial\mathbf{h}} \tag{47}$$

$\mathbf{T}^{\mathrm{AO}}$ is "unrelaxed" because it does not include changes of the RI-RPA correlation energy due to the dependence of $\mathbf{C}$ and $\boldsymbol{\varepsilon}$ on the one-particle Hamiltonian $\mathbf{h}$. $\mathbf{D}^{\mathrm{RIRPA}}$ provides access to RI-RPA one-particle properties, such as electrostatic moments and populations; natural orbitals and occupation numbers may be obtained by diagonalization of $\mathbf{D}^{\mathrm{RIRPA}}$.

Defining the AO-transformed total spin Lagrange multiplier

$$\mathbf{W}^{\mathrm{AO}} = \sum_{\sigma}\mathbf{C}_{\sigma}\mathbf{W}_{\sigma}\mathbf{C}^{\mathrm{T}}_{\sigma} \tag{48}$$

Equation 42 implies that $\mathbf{W}^{\mathrm{AO}}$ is the so-called energy-weighted total spin one-particle density matrix, that is, the total derivative of E^{RIRPA} with respect to the overlap matrix $\mathbf{S}$,

$$\mathbf{W}^{\mathrm{AO}} = -\left(\frac{\partial L^{\mathrm{RIRPA}}}{\partial\mathbf{S}}\right)_{\mathrm{stat}} = -\frac{\mathrm{d}E^{\mathrm{RIRPA}}(\mathbf{C},\boldsymbol{\varepsilon}|\mathbf{X})}{\mathrm{d}\mathbf{S}} \tag{49}$$

Finally, the four-, three-, and two-index relaxed two-particle density matrices are

$$\begin{aligned} \Gamma^{(4)}_{\kappa\lambda\mu\nu} &= \frac{\mathrm{d}E^{\mathrm{RIRPA}}(\mathbf{C},\boldsymbol{\varepsilon}|\mathbf{X})}{\mathrm{d}\Pi^{(4)}_{\mu\nu\kappa\lambda}} = \left(\frac{\partial L^{\mathrm{RIRPA}}}{\partial\Pi^{(4)}_{\mu\nu\kappa\lambda}}\right)_{\mathrm{stat}} \\ &= \sum_{\sigma\sigma'}\left(D_{\mu\nu\sigma}\left(D^{\Delta\mathrm{AO}}_{\kappa\lambda\sigma'} + \frac{1}{2}D_{\kappa\lambda\sigma'}\right) - \frac{1}{2}D_{\mu\kappa\sigma}D_{\nu\lambda\sigma'}\delta_{\sigma\sigma'}\right) \end{aligned} \tag{50}$$

$$\begin{aligned} \Gamma^{(3)}_{P\mu\nu} &= \frac{\mathrm{d}E^{\mathrm{RIRPA}}(\mathbf{C},\boldsymbol{\varepsilon}|\mathbf{X})}{\mathrm{d}\Pi^{(3)}_{\mu\nu P}} = \left(\frac{\partial L^{\mathrm{RIRPA}}}{\partial\Pi^{(3)}_{\mu\nu P}}\right)_{\mathrm{stat}} \\ &= 2\sum_{ia\sigma} C_{\mu i\sigma}C_{\nu a\sigma}\int_{-\infty}^{+\infty}\frac{\mathrm{d}\omega}{2\pi}(\mathbf{GB}\tilde{\mathbf{Q}}(\boldsymbol{\Lambda}^{-1})^{\mathrm{T}})_{ia\sigma P} \end{aligned} \tag{51}$$

dx.doi.org/10.1021/ct4008553 | J. Chem. Theory Comput. 2014, 10, 180−194

(1) Canonical $\phi_{p\sigma}$, $\varepsilon_{p\sigma}$ from KS-SCF calculation
(2) $\Delta_{ia\sigma} \leftarrow \varepsilon_{a\sigma} - \varepsilon_{i\sigma}$
(3) Compute Λ_{PQ}, Λ^{-1}_{PQ}
(4) Compute $B_{ia\sigma P}$, $B_{ij\sigma P}$ and store on disk in blocks I (Ref. 67)
(5) Determine frequency grid points ω_α and weights w_α (Ref. 45)
(6) Unrelaxed density matrix $\mathbf{T}$, accumulate $\mathbf{G}\tilde{\mathbf{Q}}$ on disk
  Loop ω_α
    Loop σ
      Loop I
        $G_{ia\sigma}(\omega_\alpha) \leftarrow \Delta_{ia\sigma}/(\Delta^2_{ia\sigma} + \omega^2_\alpha)$
        $Q_{PQ}(\omega_\alpha) \leftarrow 2B_{ia\sigma P}G_{ia\sigma}(\omega_\alpha)B_{ia\sigma Q}$
    Compute Cholesky factor $\mathbf{L}(\omega_\alpha)$ of $(\mathbf{1}_{\text{aux}} + \mathbf{Q}(\omega_\alpha))^{-1}$
    $\tilde{Q}_{PQ}(\omega_\alpha) \leftarrow L^{-1}_{PR}(\omega_\alpha)L^{-1}_{RQ}(\omega_\alpha) - \delta_{PQ}$
    $\mathtt{QQt}_{PQ} \leftarrow -(w_\alpha/4\pi)Q_{PR}(\omega_\alpha)\tilde{Q}_{RQ}(\omega_\alpha)$ (for $\mathbf{\Gamma}^{(2)}$)
    Loop σ
      Loop I
        $\mathtt{GBQt}_{ia\sigma P}(\omega_\alpha) \leftarrow G_{ia\sigma}(\omega_\alpha)B_{ia\sigma Q}\tilde{Q}_{QP}(\omega_\alpha)$
        $\mathtt{Int2GBQt}_{ia\sigma P} \leftarrow 2(w_\alpha/2\pi)\mathtt{GBQt}_{ia\sigma P}(\omega_\alpha)$
        $T_{ab\sigma} \leftarrow -[\mathbf{GBQt}(\omega_\alpha)\mathbf{B}^{\mathrm{T}}\mathbf{G}(\omega_\alpha)]_{ia\sigma ib\sigma}$
        $T_{ab\sigma} \leftarrow \omega^2_\alpha[\mathbf{\Delta}^{-1}\mathbf{GBQt}\mathbf{B}^{\mathrm{T}}\mathbf{G}\mathbf{\Delta}^{-1}]_{ia\sigma ib\sigma}$
        Loop J≤I
          $T_{ij\sigma} \leftarrow [\mathbf{GBQt}(\omega_\alpha)\mathbf{B}^{\mathrm{T}}\mathbf{G}(\omega_\alpha)]_{ia\sigma ja\sigma}$
          $T_{ij\sigma} \leftarrow -\omega^2[\mathbf{\Delta}^{-1}\mathbf{GBQt}(\omega_\alpha)\mathbf{B}^{\mathrm{T}}\mathbf{G}(\omega_\alpha)\mathbf{\Delta}^{-1}]_{ia\sigma ja\sigma}$
(7) $\boldsymbol{\gamma}$ and $\mathbf{\Gamma}$ terms
  Loop σ
    Loop I
      $\mathtt{GL}_{ib\sigma P} \leftarrow \mathtt{Int2GBQt}_{ib\sigma Q}\Lambda^{-1}_{PQ}$
      $\mathtt{GC}_{iv\sigma P} \leftarrow \mathtt{GL}_{ib\sigma P}C_{vb\sigma}$
      $\gamma_{ia\sigma} \leftarrow \mathtt{GC}_{iv\sigma P}(\mu\nu|P)C_{\mu a\sigma}$
      ⋮
      $dE/d\xi \leftarrow \mathtt{GC}_{iv\sigma P}C_{\mu i\sigma} * d\Pi^{(3)}_{\mu\nu P}/d\xi$ #$\Gamma^{(3)}$ term
      Loop J
        $\gamma_{ij\sigma} \leftarrow \mathtt{GC}_{iv\sigma P}(\mu\nu|P)C_{\mu j\sigma}$
      $\gamma_{ab\sigma} \leftarrow \mathtt{Int2GBQt}_{ia\sigma P}B_{ib\sigma P}$
      $\gamma_{aj\sigma} \leftarrow \mathtt{Int2GBQt}_{ia\sigma P}B_{ij\sigma P}$
(8) $\mathbf{\Gamma}^{(2)}$ term
  $\Gamma^{(2)}_{PQ} \leftarrow \Lambda^{-1}_{PR}\mathtt{QQt}_{RS}\Lambda^{-1}_{QS}$
  $dE/d\xi \leftarrow \Gamma^{(2)}_{PQ} * d\Pi^{(2)}_{PQ}/d\xi$
(9) Right-hand side $\mathbf{R}$
  $T^{\mathrm{AO}}_{\mu\nu\sigma} \leftarrow C_{\mu i\sigma}T_{ij\sigma}C_{\nu j\sigma} + C_{\mu a\sigma}T_{ab\sigma}C_{\nu b\sigma}$
  $R^{\mathrm{AO}}_{\mu\nu\sigma} \leftarrow H^{+,\mathrm{AO\text{-}RI}}_{\mu\nu\sigma\kappa\lambda\sigma'}T^{\mathrm{AO}}_{\kappa\lambda\sigma'} + 2F^{\mathrm{HF,RI}}_{\mu\nu\sigma}$
  $R_{ia\sigma} \leftarrow C_{\mu i\sigma}R^{\mathrm{AO}}_{\mu\nu\sigma}C_{\nu a\sigma} + \gamma_{ia\sigma} - \gamma_{ai\sigma}$
(10) Solve $\mathbf{Z}$ vector equation → $\mathbf{Z}$
(11) Lagrange multiplier $\mathbf{W}$
  $D^{\Delta\mathrm{AO}}_{\mu\nu\sigma} \leftarrow C_{\mu i\sigma}Z_{ia\sigma}C_{\nu a\sigma} + C_{\mu a\sigma}Z_{ia\sigma}C_{\nu i\sigma}$
  $D^{\Delta\mathrm{AO}}_{\mu\nu\sigma} \leftarrow C_{\mu i\sigma}T_{ij\sigma}C_{\nu j\sigma} + C_{\mu a\sigma}T_{ij\sigma}C_{\nu b\sigma}$
  $\tilde{W}^{\mathrm{AO}}_{\mu\nu\sigma} \leftarrow H^{+,\mathrm{AO\text{-}RI}}_{\mu\nu\sigma\kappa\lambda\sigma'}D^{\Delta\mathrm{AO}}_{\kappa\lambda\sigma'} + 2F^{\mathrm{HF,RI}}_{\mu\nu\sigma}$
  $W_{ij\sigma} \leftarrow C_{\mu i\sigma}\tilde{W}^{\mathrm{AO}}_{\mu\nu\sigma}C_{\nu j\sigma} + 1/2\gamma_{ij\sigma} + T_{ij\sigma}\varepsilon_{j\sigma}$
  $W_{ab\sigma} \leftarrow 1/2\gamma_{ab\sigma} + T_{ab\sigma}\varepsilon_{b\sigma}$
  $W_{ai\sigma} \leftarrow 1/2\gamma_{ai\sigma} + Z_{ai\sigma}\varepsilon_{i\sigma}$
  $W^{\mathrm{AO}}_{\mu\nu} \leftarrow C_{\mu a\sigma}W_{ai\sigma}C_{\nu i\sigma} + C_{\mu i\sigma}W_{ai\sigma}C_{\nu a\sigma}$
  $W^{\mathrm{AO}}_{\mu\nu} \leftarrow C_{\mu i\sigma}W_{ij\sigma}C_{\nu j\sigma} + C_{\mu a\sigma}W_{ab\sigma}C_{\nu b\sigma}$
(12) Add remaining contributions to the gradients
  $dE/d\xi \leftarrow (D_{\mu\nu\sigma} + D^{\Delta\mathrm{AO}}_{\mu\nu\sigma}) * dh_{\mu\nu\sigma}/d\xi$
  $\tilde{D}_{\mu\nu\sigma} \leftarrow D^{\Delta\mathrm{AO}}_{\mu\nu\sigma} + D_{\mu\nu\sigma}$
  $dE/d\xi \leftarrow (D_{\mu\nu\sigma}\tilde{D}_{\kappa\lambda\sigma'} - 1/2D_{\mu\kappa\sigma}D_{\nu\lambda\sigma'}\delta_{\sigma\sigma'}) * d(\mu\nu|\kappa\lambda)_{\mathrm{RI}}/d\xi$
  $dE/d\xi \leftarrow D^{\Delta\mathrm{AO}}_{\mu\nu\sigma} * \partial V^{\mathrm{XC}}[\mathbf{D}]/\partial\xi$
  $dE/d\xi \leftarrow W^{\mathrm{AO}}_{\mu\nu} * dS_{\mu\nu}/d\xi$

Figure 1. Algorithm for final gradients, which uses array blocks $\{i,a,P\}$ containing $i \in I$ where I is a subset of occupied MOs and a, P for all virtual MOs and auxiliary functions. Operator ← accumulates indices appearing on the right-hand side if they do not appear on the left. Index loops are implicit if not explicitly shown. ω_α and w_α represent frequency grid points and quadrature weights. 3-index MO arrays are stored on disk while all 3-index AO arrays are directly computed. "RI" indicates computation with 3-index AO integrals using the RI approximation.

$$\Gamma^{(2)}_{\mathrm{QP}} = \frac{\mathrm{d}E^{\mathrm{RIRPA}}(\mathbf{C}, \boldsymbol{\varepsilon}|\mathbf{X})}{\mathrm{d}\Pi^{(2)}_{\mathrm{PQ}}} = \left(\frac{\partial L^{\mathrm{RIRPA}}}{\partial \Pi^{(2)}_{\mathrm{PQ}}}\right)_{\mathrm{stat}}$$
$$= -\frac{1}{2}\int_{-\infty}^{+\infty}\frac{\mathrm{d}\omega}{2\pi}(\mathbf{\Lambda}^{-1}\mathbf{Q}\tilde{\mathbf{Q}}(\mathbf{\Lambda}^{-1})^{\mathrm{T}})_{\mathrm{PQ}} \quad (52)$$

The results of this section illustrate once more a key advantage of the Lagrangian method: *Total* RI-RPA energy derivatives featuring a complicated implicit dependence on the parameter $\mathbf{X}$ through the variables $\mathbf{C}$ and $\boldsymbol{\varepsilon}$ are replaced by *partial* derivatives of the RI-RPA Lagrangian, whose computation is straightforward once the stationary point of the Lagrangian has been fully determined.

2.5. Implementation. For applications such as geometry optimizations or molecular dynamics, it is most important that the computational time required for the energy gradients with respect to all molecular coordinates is on the order of a single point energy calculation. The algorithm for the computation of RI-RPA gradients is displayed in Figure 1. The rate-determining steps of this algorithm are highlighted in the following. In step 10, the $\mathbf{Z}$ vector equation is solved in an integral direct fashion using iterative subspace methods,[64,65] the RI-J approximation, and Schwarz screening of ERIs. Since the number of $\mathbf{Z}$ vector iterations is approximately independent of the system size, this step scales as $O(N^2)$ (besides some fast cubic scaling linear algebra steps). The overall rate-determining step in the calculation is step 6 with an asymptotic $O(N^4 \log N)$ scaling of the operation count. Tests on *n*-alkanes using quadruple-ζ basis sets[66] produced CPU times for nuclear gradient calculations ∼5 times that of a single point RPA energy calculation, independent of system size.

While low floating point operation counts are important for performance, they should go together with an affordable memory and disk storage consumption. The latter may increase with the number of "non-separable" indices in the algorithm, for example, the number of indices appearing in each integral, which is not factorized. In the present algorithm, there are at most 3-index quantities. The 3-index AO integrals are directly computed, while 3-index MO integrals are entirely stored on disk. Among the latter, the ERIs $B_{ia\sigma P}$ (step 4) and the frequency-integrated contributions $\mathrm{Int2GBQt}_{ia\sigma P}$ (step 6) are the most storage-consuming arrays. Thus, the required storage scales as $O(N_{\mathrm{occ}} \times N_{\mathrm{virt}} \times N_{\mathrm{aux}})$. For larger systems, the occupied MOs may be partitioned into blocks depending on the amount of memory available.

Although RPA is not perturbative, it is helpful to compare RI-RPA with MP2 methods to analyze its computational complexity. The implementation of the RI-RPA gradients has some reminiscence of RI-MP2 gradients.[67] A major difference is the loop over frequency grid points, which is not present in the RI-MP2 implementation. The frequency integration in RI-RPA entirely avoids 4-index arrays, in contrast to conventional RI-MP2. The scaling for RI-RPA, $O(N^4 \log N)$, is thus lower than the $O(N^5)$ scaling of RI-MP2, and the storage of 4-index arrays either in memory or on disk is entirely avoided. On the other hand, RI-RPA uses a numerical quadrature to achieve additional factorization and thus could also be compared to scaled opposite-spin Laplace transform RI-MP2,[68] which scales as

dx.doi.org/10.1021/ct4008553 | J. Chem. Theory Comput. 2014, 10, 180−194

Table 2. Predicted Equilibrium Bond Distances r_e (pm) and Angles α (deg) Displayed as Differences from the Reference Values, Including Mean Absolute Errors (MAE), Mean Signed Errors (MSE), and Absolute Maximum Errors (Max)[a]

	param.	ref[b]	RPA	MP2	PBE	PBE0
H_2	r_e	74.1491	0.14	−0.55	0.82	0.31
F_2	r_e	141.268	2.23	−1.79	0.05	−3.76
N_2	r_e	109.773	0.63	1.09	0.43	−0.91
HF	r_e	91.6879	0.33	−0.01	1.32	0.09
CO	r_e	112.836	0.71	0.43	0.70	−0.61
CO_2	r_e	116.006	0.64	0.38	1.04	−0.41
HCN	r_e(CH)	106.528	0.13	−0.27	0.96	0.25
	r_e(CN)	115.336	0.51	0.77	0.41	−0.87
HNC	r_e(NH)	99.489	0.06	−0.06	1.01	0.12
	r_e(CN)	116.875	0.64	0.22	0.60	−0.62
C_2H_2	r_e(CH)	106.166	0.03	−0.68	0.84	0.21
	r_e(CC)	120.356	0.17	0.92	0.30	−0.77
H_2O	r_e	95.7902	0.33	−0.10	1.09	−0.03
	α	104.4	−0.47	−0.08	−0.19	0.49
HNO	r_e(HN)	105.199	0.15	−0.48	2.77	0.80
	r_e(NO)	120.859	0.68	0.50	−0.17	−1.90
	α	108.26	−0.03	−0.31	0.50	0.62
HOF	r_e(HO)	96.8619	0.16	−0.31	1.10	−0.21
	r_e(OF)	143.447	2.11	−1.44	1.04	−2.88
	α	97.86	−0.63	0.24	0.17	1.30
N_2H_2	r_e(NH)	102.883	0.21	−0.32	1.47	0.24
	r_e(NN)	124.575	0.48	0.10	0.01	−1.65
	α	106.34	−2.80	−1.97	−2.55	−1.65
CH_2O	r_e(CH)	110.072	0.12	−0.34	1.63	0.65
α(HCO)	r_e(CO)	120.465	0.49	0.16	0.30	−0.98
	α	121.63	0.18	0.11	0.40	0.32
C_2H_4	r_e(CH)	108.068	0.12	−0.31	1.01	0.28
α(HCC)	r_e(CC)	133.074	0.16	−0.50	0.15	−0.83
	α	121.4	0.15	−0.01	0.32	0.26
NH_3	r_e	101.139	0.26	−0.37	0.96	0.01
	α	107.17	−1.01	−0.08	−0.88	−0.22
CH_4	r_e	108.588	0.18	−0.40	0.93	0.25
H_2S	r_e	133.56[c]	0.11	−0.65	1.55	0.45
	α	92.11[c]	−0.03	0.02	−0.42	0.14
MAE	r_e		0.45	0.51	0.87	0.77
MSE	r_e		0.45	−0.15	0.86	−0.49
Max	r_e		2.23	1.79	2.77	3.76
MAE	α		0.66	0.35	0.68	0.63
Max	α		2.80	1.97	2.55	1.65

[a]Calculated structures were optimized with QZVPPD basis sets. [b]Taken from ref 89, obtained from least-squares fits involving experimental rotational constants and CCSD(T)/cc-pVQZ rotation-vibration interaction constants. [c]Taken from ref 90, obtained from infrared and microwave spectroscopy combined with a force field model.

$O(N^4)$, and other low-scaling Laplace transform MP2 methods.[69−74] The first-order properties developed in this work have been implemented in the TURBOMOLE program package[75,76] and will be released in version 6.6.

3. RESULTS

3.1. Computational Details. The MP2 and RPA calculations were based on self-consistent HF and KS orbitals, respectively; the Generalized Gradient Approximation (GGA) functional PBE[9] was used to generate the latter. Semilocal DFT calculations using the PBE and PBE0[77] functionals were performed for comparison. In the self-consistent field calculations, ground state energies and one-particle density matrices were converged to at least 10^{-7} au. Large grids (size 5) were employed throughout.[78] The number of frequency grid points used to compute the RPA correlation contributions was selected to ensure a sensitivity measure of no more than 3×10^{-4}. This sensitivity measure is an estimate for the accuracy of the RI-RPA energy; see Supporting Information. For vibrational frequencies, the sensitivity measure did not exceed 10^{-7} and structures were reoptimized with larger frequency grids. The RI-J approximation and corresponding auxiliary basis sets[79−81] were used for all calculations. For HF and MP2 calculations, the RI-JK algorithm and the corresponding optimized auxiliary basis sets were applied.[82] Throughout this work, Dunning's (augmented) correlation-consistent basis sets[83−85] are denoted (aug)-cc-pVXZ where X = T, Q. Core weighted functions (aug-cc-pwCVQZ) were used for all-electron calculations. In addition, quadruple-ζ basis sets with augmented polarization functions[66] (QZVPP) and the corresponding property-optimized basis sets[86] (QZVPPD) were employed. DFT[87] and MP2[88] methods were used within

dx.doi.org/10.1021/ct4008553 | J. Chem. Theory Comput. 2014, 10, 180−194

Table 3. Predicted Equilibrium Bond Distances r_e (pm) Displayed as Differences from the Experimental Values, Including Mean Absolute Errors (MAE), Mean Signed Errors (MSE), and Absolute Maximum Errors (Max)[a]

	bond type	exp.[b]	RPA	MP2	PBE	PBE0
$Ni(CO)_4$	Ni−C	183.6	−1.14	−6.36	−1.16	−1.42
	C−O	114.0	0.21	0.58	0.76	−0.85
$Fe(CO)_5$	$(Fe-C)_{av}$	182.9	−2.09	−9.99	−2.47	−3.06
	$(C-O)_{ax}$	114.1	0.33	2.34	0.94	−0.75
	$(C-O)_{eq}$	114.8	−0.06	0.25	0.51	−1.09
$FeCp_2$	Fe−C	206.4	−2.65	−16.88	−1.87	−1.81
MAE			1.08	6.07	1.28	1.50
MSE			−0.90	−5.01	−0.55	−1.50
Max			2.65	16.88	2.47	3.06

[a]Calculated structures were optimized with QZVPP basis sets. Abbreviations: av = mean value of axial and equatorial bond distances, ax = axial, eq = equatorial, Cp = Cyclopentadienyl. [b]Taken from ref 97 ($Ni(CO)_4$), ref 108 ($Fe(CO)_5$), and ref 91 ($FeCp_2$; see also ref 109).

TURBOMOLE version 6.5[75,76] RPA forces for structure optimizations and RPA dipole moments were computed analytically using eq 42. Harmonic vibrational frequencies were computed from finite differences of analytical RPA gradients.

3.2. Equilibrium Structures. The quality of RPA equilibrium structures was assessed using the reference values of Pawłowski et al. for 17 small molecules[89] (Table 2) and Cook for H_2S.[90] These values are believed to be accurate within 0.08 pm. Pawłowski et al. obtained the equilibrium structures from experimental rotational constants and calculated vibration−rotation interaction constants, while Cook determined the H_2S structure using experimental infrared and microwave data combined within the theoretical framework of the small oscillations model. The RPA bond lengths have a mean absolute error (MAE) of 0.45 pm, with the largest errors arising for F−F and O−F bonds, whose lengths are overestimated by 2.2 and 2.1 pm, respectively. With an MAE of 0.51 pm, errors in the MP2 bond lengths are slightly larger. PBE and the PBE0 hybrid are less accurate and consistently overestimate the bond lengths.

Except for the H_2S molecule, the identical test set was used by Rekkedal et al. to compare the MP2 and RPA(HF)/cc-pVQZ equilibrium structures.[43] While the MAE of MP2 bond

Table 5. Predicted Dipole Moments (debye) Displayed As Differences from the Experimental Values, Including Mean Absolute Errors (MAE), Mean Signed Errors (MSE), and Absolute Maximum Errors (Max)[a]

	exp.[b]	RPA	CCSD(T)[c]	MP2	PBE	PBE0
HF	1.826	−0.07	−0.04	−0.02	−0.06	−0.02
CO	0.11	0.00	0.04	0.16	0.09	0.01
H_2O	1.85	−0.04	−0.02	0.01	−0.05	0.00
NH_3	1.47	0.03	0.03	0.04	0.02	0.05
H_2S	0.97	−0.05	0.01	0.02	0.00	0.04
MAE		0.04	0.03	0.05	0.04	0.02
MSE		−0.03	0.00	0.04	0.00	0.02
Max		0.07	0.04	0.16	0.09	0.05

[a]Calculated with QZVPPD basis sets for structures from Table 2. [b]Taken from ref 110. See there also for further DFT results on dipole moments. [c]From ref 111 using experimental structures and basis sets derived from Sadlej.

Table 4. Predicted Equilibrium Intermonomer Distances (pm) Displayed as Differences from the CCSD(T) Values, Including Mean Absolute Errors (MAE), Mean Signed Errors (MSE), and Absolute Maximum Errors (Max)[a]

	CCSD(T)[b]	RPA	MP2	PBE	PBE0
(1) $H_2O\cdots NH_3$	198.50	0.20	−3.03	−6.30	−4.57
(2) $H_2O\cdots H_2O$	196.18	0.92	−2.43	−3.66	−3.11
(3) HCN···HCN	222.53	0.27	−0.04	−2.59	−3.11
(4) HF···HF	183.27	0.21	−2.04	−3.86	−3.36
(5) $NH_3\cdots NH_3$	252.42	3.68	−1.53	−0.65	0.12
(6) $HF\cdots CH_4$	231.95	5.61	−0.09	−6.11	−4.25
(7) $NH_3\cdots CH_4$	279.33	6.57	1.31	−1.14	0.52
(8) $H_2O\cdots CH_4$	262.79	6.21	0.64	−1.10	0.37
(9) HCHO···HCHO	314.54	14.74	−2.43	−8.36	−0.97
(10) $H_2O\cdots CH_2CH_2$	242.20	1.40	−6.10	−1.10	−0.20
(11) $HCHO\cdots CH_2CH_2$	346.15	0.44	−0.08	19.96	17.25
(12) CHCH···CHCH	269.30	0.30	0.50	−0.50	0.60
(13) $NH_3\cdots CH_2CH_2$	273.00	1.10	−0.20	−0.50	0.00
(14) $CH_2CH_2\cdots CH_2CH_2$	381.20	1.20	−0.30	0.50	30.70
(15) $CH_4\cdots CH_2CH_2$	312.30	0.10	0.50	−0.50	0.10
(16) $BH_3\cdots CH_4$	297.94	15.25	−0.13	−35.95	−22.02
(17) $CH_4\cdots CH_3CH_3$[c]	365.50	−0.66	−0.13	44.13	44.75
(18) $CH_4\cdots CH_3CH_3$[c]	361.95	−1.82	−0.50	40.68	42.68
(19) $CH_4\cdots CH_4$	363.80	0.10	−0.03	40.23	42.24
(20) $Ar\cdots CH_4$	367.85	−1.71	−6.65	32.30	36.02
(21) $Ar\cdots CH_2CH_2$	389.90	−2.40	−0.40	32.40	40.10
MAE		3.09	1.38	13.45	14.14
MSE		2.46	−1.10	6.56	10.18
Max		15.25	6.65	44.13	44.75

[a]Structures were optimized using QZVPPD basis sets. [b]Taken from the A24 test set in ref 98, for the complete basis set limit. [c]Conformers 17 and 18 are bent and linear, respectively, regarding the C atoms.

dx.doi.org/10.1021/ct4008553 | J. Chem. Theory Comput. 2014, 10, 180−194

Table 6. Predicted Dipole Moments (debye) Displayed as Differences from the Experimental Values, Including Mean Absolute Errors (MAE), Mean Signed Errors (MSE), and Absolute Maximum Errors (Max)

	exp.	RPA[a]	MP2[b]	PBE[a]	PBE0[a]	ref.
HF	1.826	−0.06	−0.02	−0.07	−0.02	112
CO	0.11	−0.01	0.14	0.09	−0.03	112
pyrrole	1.767	0.09	0.11	0.10	0.11	113
furan	0.685	−0.07	−0.06	−0.13	−0.07	113
HCHO···HCHO	0.858	0.08	0.23	0.45	0.36	114
H_2O···H_2O	2.6	−0.04	0.02	0.03	0.06	115
H_3N···SO_3	6.204	−0.04	−0.07	−0.07	0.06	116
MAE		0.06	0.09	0.14	0.10	
MSE		−0.01	0.05	0.06	0.07	
Max		0.09	0.23	0.45	0.36	

[a]Dipole moments for aug-cc-pwCVQZ basis sets on MP2/aug-cc-pVTZ structures. Diatomics are optimized within RPA/aug-cc-pwCVQZ. [b]For aug-cc-pVTZ basis sets.

Table 7. Predicted Harmonic Frequencies (cm^{-1}) of QZVPP-Optimized Structures Displayed As Differences from the Experimental Values, Including Mean Absolute Errors (MAE), Mean Signed Errors (MSE), and Absolute Maximum Errors (Max)

	vibration	exp.[a]	RPA	CCSD(T)[b,c]	MP2	PBE	PBE0
F_2	σ stretch	917	−47	16	88	77	179
N_2	σ stretch	2359	−19	14	−153	−9	122
HF	σ stretch	4138	−7	8	21	−164	17
CO	σ stretch	2170	−38	7	−42	−41	69
H_2O	a_1 bend	1646	3	18	−11	−53	−12
	a_1 stretch	3832	−18	26	25	−123	37
	b_1 stretch	3945	−21	21	39	−130	30
NH_3	a_1 bend	1030	46	54	13	−3	6
	e bend	1690	−29	−10	−18	−69	−25
	a_1 stretch	3503	−39	−22	20	−115	7
	e stretch	3592	2	17	80	−81	47
H_2S	a_1 bend	1215	−13	−6	1	−50	−10
	a_1 stretch	2722	−27	−6	66	−90	6
	b_1 stretch	2733	−22	−1	76	−85	9
MAE			24	16	47	78	41
MSE			−16	10	15	−67	34
Max			47	54	153	164	179

[a]Diatomics taken from ref 117, H_2O and NH_3 from ref 118, and H_2S from ref 119. [b]Basis sets used and original data: all electron basis set limit for diatomics (ref 117), cc-pVTZ for H_2O (ref 120), cc-pVQZ for NH_3 (ref 121), and aug-cc-pVQZ for H_2S (ref 122). [c]See also ref 123 for alternative CCSD(T) results of diatomics.

distances reported in ref 43 is the same as ours, 0.5 pm, the MAE of RPA(HF) from ref 43 is over three times larger than the MAE we obtain from RI-RPA(PBE). To verify that the errors reported by Rekkedal et al. are due to the use of HF instead of a KS reference, we selected the F_2 molecule and calculated its RI-RPA(HF)/QZVPPD equilibrium bond length using finite differences. Thus, we reproduced the RPA(HF)/cc-pVQZ value of 136 pm reported in Figure 2(a) of ref 43, which is over 5 pm less than the reference value of 141.3 pm. For comparison, the RI-RPA(PBE) bond distance is 143.5 pm.

Transition metal complexes pose a challenge to electronic structure methods due to small gaps and strong dynamic correlation effects. We selected three complexes where accurate experimental data are available.[91] The results in Table 3 show that RPA underestimates the bond lengths somewhat but they are accurate compared to MP2. The MP2 metal−carbon bond lengths are at least 6 pm too short. This is in line with other MP2 calculations[92−95] showing overestimation of metal−ligand interactions. The PBE and PBE0 results are comparable in accuracy to the RPA results. The maximum error of RPA is −2.65 pm for the Fe−C bonds in ferrocene. For the Fe−C bonds of the $Fe(CO)_5$ complex, mean values of axial and equatorial equilibrium bond distances were calculated because only the mean value of 182.9 pm is experimentally known with a high precision from electron diffraction data.[91] For the $Fe(CO)_5$ complex, axial and equatorial Fe−C equilibrium bond distances of 180.7 and 180.9 pm, respectively, have been calculated with RPA. The resulting RPA mean value for the Fe−C bond is −2.09 pm too short compared to the reference. Likewise, PBE and PBE0 predict too short equilibrium distances for this bond. Another gas-phase electron diffraction experiment for $Fe(CO)_5$ combined with data from vibrational spectroscopy yields axial and equatorial Fe−C bond lengths of 180.7 and 182.7 pm.[96] These values yield a better agreement with our calculated results. For the $Ni(CO)_4$ complex, the RPA-optimized Ni−C bond length is accurate within 1.2 pm, while the MP2 value is more than 6 pm too short compared to electron diffraction data.[97]

Structures of weakly bound dimers were studied for 21 systems from the A24 test set[98] (see Table 4). Dimers 1−5 are

predominantly bound by hydrogen-bonding (H-bonding), dimers 6−15 are bound by a mixture of H-bonding and dispersion interactions, and dimers 15−21 are predominantly bound by dispersion interactions. Intermonomer distances were defined as specified in the Supporting Information, and reference values were obtained from the CCSD(T)-optimized structures at the complete basis set limit.[98] We observe that RPA systematically overestimates equilibrium intermonomer distances for all types of weak interactions. This is in agreement with the underbinding found for the weakly bound diatomics[42] and dimers[16] in RPA studies using non-RPA reference structures. For complexes dominated by H-bonding, RPA deviates by 1 pm on average from reference values, while for the mixed and dispersion dominated systems a MAE of 4 pm is observed. MP2 exhibits similar performance, predicting intermonomer distances to within 2 pm on average, but equilibrium distances are generally underestimated not overestimated. For the H-bonding and mixed systems, PBE and PBE0 are less systematic, but on average, they predict the intermonomer distances to within 3−6 pm of the reference. However, for the dispersion bound systems these semilocal functionals fail catastrophically, as expected,[99,100] overestimating equilibrium intermonomer distances by at least 30 pm.

3.3. Dipole Moments. For the small benchmark systems in Table 5, the dipole moments are well-predicted by all methods with a MAE of at most 0.05 D. For molecules characterized by several electronically resonant Lewis structures including dipolar forms and weakly bound dimers, RPA provides a better description of the electronic structure compared to MP2, PBE, and PBE0, as shown in Table 6. The errors increase slightly for all methods compared to the smaller systems; however, RPA clearly outperforms the other methods here.

3.4. Harmonic Vibrational Frequencies. With a mean signed error (MSE) of −16 cm^{-1}, harmonic vibrational frequencies of small main group molecules are very accurate (see Table 7). This is in line with previous results,[27,34] and the MSE of −11 cm^{-1} calculated for the noble gas diatomics, Be_2, and Mg_2 from the data reported in ref 101. The MAE and maximum error of the RPA frequencies are also small and comparable to the CCSD(T) results. As expected,[102,103] the PBE functional underestimates harmonic vibrational frequencies, while PBE0 is more accurate but has a tendency to overcorrect PBE. The accuracy of the MP2 results is comparable to PBE0 for the present benchmark.

4. CONCLUSION

The results of this paper suggest that RPA structures are significantly more accurate than MP2 structures, especially for small-gap systems. With our $O(N^4 \log N)$ scaling implementation, the computational cost of a RI-RPA geometry optimization becomes comparable to that of a RI-MP2 geometry optimization. Thus, RI-RPA emerges as a valuable tool for predicting minima and transition state structures of open-shell d- and f-element compounds, particularly when semilocal functionals produce wildly varying results. Being robust, nonempirical, and relatively inexpensive, RI-RPA possesses many desirable features of a general purpose method that can be applied indiscriminately to a wide range of different systems and chemical environments.

The vast improvement over MP2 for small-gap systems depends on the use of a noninteracting KS reference rather than HF[43] in RPA calculations. This is in line with previous observations[104] that HF-based direct RPA performs poorly for energy differences. The remaining dependence on the semilocal functional used for the KS calculation is mostly small compared to typical RPA errors but could be reduced further by orbital optimization. The Lagrangian technique developed here lays the groundwork for such a self-consistent RPA, without the need to invoke optimized effective potential (OEP) theory.[105−107] Orbital optimization also help address some of the underbinding we observe in RPA calculations of weakly bound complexes.

From a computational point of view, the present RI implementation combined with imaginary frequency integration greatly improves upon the $O(N^6)$ scaling of RPA analytical gradients based on ring-CCD:[43] analytical RI-RPA gradients are ∼5 times more expensive than a single-point RI-RPA energy, independent of system size. Thus, RI-RPA geometry optimizations for molecules in the 100 atoms range are now well within reach.

APPENDIX A

Equations for the Lagrange Multipliers D^Δ and W

Using the Lagrangian and energy definitions 21 and 8, the stationarity condition 24 determines the occupied−occupied and virtual−virtual parts of the difference density matrix $\mathbf{D}^\Delta$,

$$\left(\frac{\partial L^{\mathrm{RIRPA}}}{\partial \mathcal{E}_{ij\sigma}}\right)_{\mathrm{stat}} = \left(\frac{\partial E^{\mathrm{RIRPA}}}{\partial \mathcal{E}_{ij\sigma}}\right)_{\mathrm{stat}} - D^\Delta_{ij\sigma} = 0$$

similarly, we obtain

$$D^\Delta_{ab\sigma} = \left(\frac{\partial E^{\mathrm{RIRPA}}}{\partial \mathcal{E}_{ab\sigma}}\right)_{\mathrm{stat}} \tag{53}$$

The partial derivatives of E^{RIRPA} are evaluated in the following, using the short hand notation $(\partial/\partial\mathcal{E}_{ij\sigma})_{\mathrm{stat}} \equiv {}'$:

$$(E^{\mathrm{RIRPA}})' = (E^{\mathrm{C\,RIRPA}})' = \frac{1}{2}\int_{-\infty}^{\infty}\frac{\mathrm{d}\omega}{2\pi}\langle\tilde{\mathbf{Q}}\mathbf{Q}'\rangle \tag{54}$$

where the derivative of $\mathbf{Q}$ from eq 14 is

$$\mathbf{Q}' = 2\mathbf{B}^{\mathrm{T}}\mathbf{G}'\mathbf{B} \tag{55}$$

The derivative of matrix $\mathbf{G}$ from eq 15 is

$$\mathbf{G}' = \mathbf{\Delta}'\mathbf{\Delta}^{-1}\mathbf{G} - \mathbf{G}\mathbf{\Delta}'\mathbf{G} - \mathbf{G}\mathbf{\Delta}\mathbf{\Delta}'\mathbf{\Delta}^{-1}\mathbf{G} \tag{56}$$

with the derivative of matrix $\mathbf{\Delta}$, eq 16,

$$\Delta'_{kc\sigma' ld\sigma''} = -\delta_{\sigma'\sigma''}\delta_{\sigma\sigma''}\delta_{ki}\delta_{lj}\delta_{cd} \tag{57}$$

Inserting the intermediate results 55, 56, and 57 into eq 54 and using $\mathbf{1} - \mathbf{G}\mathbf{\Delta} = \omega^2\mathbf{G}\mathbf{\Delta}^{-1}$, we arrive at the final result

$$D^\Delta_{ij\sigma} = \left(\frac{\partial E^{\mathrm{RIRPA}}}{\partial \mathcal{E}_{ij\sigma}}\right)_{\mathrm{stat}} = T_{ij\sigma} \tag{58}$$

and similarly

$$D^\Delta_{ab\sigma} = T_{ab\sigma} \tag{59}$$

where $T_{ij\sigma}$ and $T_{ab\sigma}$ are given by eqs 29 and 30.

In the next step, the orbital derivatives $\sum_\mu (\partial L^{\mathrm{RIRPA}}/\partial C_{\mu p\sigma})_{\mathrm{stat}} C_{\mu q\sigma}$ from stationarity condition 25 determine the off-diagonal parts of $\mathbf{D}^\Delta$ and the entire $\mathbf{W}$. Using the shorthand notation

dx.doi.org/10.1021/ct4008553 | J. Chem. Theory Comput. 2014, 10, 180−194

$\sum_\mu (\partial/\partial C_{\mu p\sigma})_{\mathrm{stat}} C_{\mu q\sigma} \equiv {}'$, the expression for orbital derivatives is given by

$$(L^{\mathrm{RIRPA}})' = 0 = \langle\Phi|\hat{H}|\Phi\rangle' + (E^{\mathrm{C\,RIRPA}})' + \sum_{rs\sigma'} D^{\Delta}_{rs\sigma'}(\varepsilon_{rs\sigma'})' - \sum_{rs\sigma'} W_{rs\sigma'}\langle r\sigma'|s\sigma'\rangle' \tag{60}$$

From eq 9, the derivatives of the HF energy functional follow as [cf. eq 38]

$$\langle\Phi|\hat{H}|\Phi\rangle' = 2\sum_k \delta_{pk}[\langle q\sigma|\hat{h}|k\sigma\rangle + \sum_{j\sigma'} (kq\sigma|jj\sigma') - \sum_j (qj\sigma|kj\sigma)] = 2\sum_k \delta_{pk}\varepsilon^{\mathrm{HF}}_{pq\sigma} \tag{61}$$

The derivatives of the correlation energy, eq 10, required in eq 60 are already given by the right hand side of expression 54 replacing the derivative of $\mathbf{Q}'$ with

$$\mathbf{Q}' = 2((\mathbf{B}')^{\mathrm{T}}\mathbf{G}\mathbf{B} + \mathbf{B}^{\mathrm{T}}\mathbf{G}\mathbf{B}') \tag{62}$$

and

$$B'_{kc\sigma' P} = \delta_{\sigma\sigma'}[\delta_{pk}B_{qc\sigma' P} + \delta_{pc}B_{kq\sigma' P}] \tag{63}$$

The final result for the correlation energy part is

$$\sum_\mu \left(\frac{\partial E^{\mathrm{C\,RIRPA}}}{\partial C_{\mu p\sigma}}\right)_{\mathrm{stat}} C_{\mu q\sigma} = \gamma_{pq\sigma} \tag{64}$$

The orbital derivatives of KS matrix elements in eq 60 are

$$\varepsilon'_{rs\sigma'} = \delta_{\sigma\sigma'}(\delta_{pr}\varepsilon_{qs\sigma} + \delta_{ps}\varepsilon_{rq\sigma}) + 2\sum_k \delta_{pk}[(rs\sigma'|pq\sigma) + f^{\mathrm{XC}}_{rs\sigma' pq\sigma}] \tag{65}$$

with the XC kernel from eq 35. Using this equation, the one-particle difference density matrix term is

$$\sum_{rs\sigma'} D^{\Delta}_{rs\sigma'}\varepsilon'_{rs\sigma'} = 2(\mathbf{D}^{\Delta}_\sigma\boldsymbol{\varepsilon}_\sigma)_{pq} + \sum_k \delta_{pk}(\mathbf{H}^{+}\mathbf{D}^{\Delta})_{pq\sigma} \tag{66}$$

Finally, the derivative of the energy-weighted one-particle density matrix term in eq 60 is

$$\sum_{rs\sigma'} W_{rs\sigma'}\langle r\sigma'|s\sigma'\rangle' = 2W_{pq\sigma} \tag{67}$$

Equations 61, 64, 66, and 67 are used in the derivative 60 yielding the following result for the stationarity eq 25,

$$2W_{ij\sigma} = Q_{ij\sigma} + (\mathbf{H}^{+}\mathbf{Z})_{ij\sigma} \tag{68}$$

$$2W_{ia\sigma} = Q_{ia\sigma} + 2(\mathbf{Z}_\sigma\boldsymbol{\varepsilon}_\sigma)_{ia} + (\mathbf{H}^{+}\mathbf{Z})_{ia\sigma} \tag{69}$$

$$2W_{ai\sigma} = 2W_{ia\sigma} = Q_{ai\sigma} + 2(\mathbf{Z}_\sigma\boldsymbol{\varepsilon}_\sigma)_{ai} \tag{70}$$

$$2W_{ab\sigma} = Q_{ab\sigma} \tag{71}$$

with

$$Q_{ij\sigma} = \gamma_{ij\sigma} + 2\varepsilon^{\mathrm{HF}}_{ij\sigma} + 2(\mathbf{T}_\sigma\boldsymbol{\varepsilon}_\sigma)_{ij} + (\mathbf{H}^{+}\mathbf{T})_{ij\sigma} \tag{72}$$

$$Q_{ia\sigma} = \gamma_{ia\sigma} + 2\varepsilon^{\mathrm{HF}}_{ia\sigma} + (\mathbf{H}^{+}\mathbf{T})_{ia\sigma} \tag{73}$$

$$Q_{ai\sigma} = \gamma_{ai\sigma} \tag{74}$$

$$Q_{ab\sigma} = \gamma_{ab\sigma} + 2(\mathbf{T}_\sigma\boldsymbol{\varepsilon}_\sigma)_{ab} \tag{75}$$

Equations 68 to 75 are given for non-canonical orbitals. $\mathbf{D}^{\Delta}$ was split into $\mathbf{T}$ and $\mathbf{Z}$ [cf. eq 28] and vanishing occupied−virtual/virtual−occupied blocks were employed for $\boldsymbol{\varepsilon}$. Further, the symmetry of the energy-weighted density matrix, $W_{ia\sigma} = W_{ai\sigma}$, yields the $\mathbf{Z}$ vector equation, eq 33.

APPENDIX B

Quadrature Weight Derivatives

Replacing the frequency integrals by sums over finite frequency grids, that is,

$$\int_{-\infty}^{\infty} \mathrm{d}\omega f(\omega) \to \sum_{\alpha=1}^{N_{\mathrm{g}}} w_\alpha f(\omega_\alpha) \tag{76}$$

throughout the Lagrangian defined in eq 21, an augmented Lagrangian may be defined,

$$\begin{aligned} L^{\mathrm{RIRPA}}_{\mathrm{g}}(\boldsymbol{C}, \boldsymbol{\mathcal{E}}, \mathcal{A}, \mathcal{T}, \boldsymbol{\mathcal{D}}^{\Delta}, \boldsymbol{\mathcal{W}}|\mathbf{X}, \mathbf{V}^{\mathrm{XC}}, \mathbf{S}) &= E^{\mathrm{RIRPA}}_{\mathrm{g}}(\boldsymbol{C}, \boldsymbol{\mathcal{E}}, \mathcal{A}|\mathbf{X}) \\ &+ \mathcal{T}(E^{\mathrm{d}}(\boldsymbol{C}, \boldsymbol{\mathcal{E}}|\mathbf{X}) - E^{\mathrm{d}}_{\mathrm{g}}(\boldsymbol{C}, \boldsymbol{\mathcal{E}}, \mathcal{A})|\mathbf{X}) \\ &+ \sum_\sigma (\langle\boldsymbol{\mathcal{D}}^{\Delta}_\sigma(\boldsymbol{C}^T_\sigma\mathbf{F}_\sigma\boldsymbol{C}_\sigma - \boldsymbol{\mathcal{E}}_\sigma)\rangle - \langle\boldsymbol{\mathcal{W}}_\sigma(\boldsymbol{C}^T_\sigma\mathbf{S}\boldsymbol{C}_\sigma - \mathbf{1})\rangle) \end{aligned} \tag{77}$$

where the subscript "g" denotes terms computed on the grid. $L^{\mathrm{RIRPA}}_{\mathrm{g}}$ contains an additional constraint

$$E^{\mathrm{d}} = E^{\mathrm{d}}_{\mathrm{g}}(\mathcal{A}) \tag{78}$$

and an additional Lagrange multiplier $\mathcal{T}$, since the frequency grid depends on the perturbation ξ. For a given number of grid points, N_{g}, the scaling parameter $\mathcal{A}$ completely determines the grid points ω_α and the quadrature weights w_ω

$$\omega_\alpha = \mathcal{A}\omega_{\mathrm{u}\alpha}(N_{\mathrm{g}}) \quad \text{and} \quad w_\alpha = \mathcal{A}w_{\mathrm{u}\alpha}(N_{\mathrm{g}}) \tag{79}$$

where the unscaled values $w_{\mathrm{u}\alpha}$ and $\omega_{\mathrm{u}\alpha}$ were defined in ref 45. In the constraint 78, E^{d} and $E^{\mathrm{d}}_{\mathrm{g}}$ are approximations of the correlation energy $E^{\mathrm{C\,RIRPA}}$. E^{d} and $E^{\mathrm{d}}_{\mathrm{g}}$ were derived from the exact expression[45]

$$E^{\mathrm{C\,RIRPA}} = \frac{1}{2}\int\frac{\mathrm{d}\omega}{2\pi}\langle\ln[(\omega^2\mathbf{1} + \boldsymbol{\Omega}^2) \times (\omega^2\mathbf{1} + (\mathbf{U}^{(0)})^{-1}\boldsymbol{\Delta}^2\mathbf{U}^{(0)})^{-1}] - 2\boldsymbol{\Delta}^{1/2}\mathbf{B}\mathbf{B}^{\mathrm{T}}\boldsymbol{\Delta}^{1/2}(\omega^2\mathbf{1} + \boldsymbol{\Delta}^2)^{-1}\rangle \tag{80}$$

where $\boldsymbol{\Omega}^2$ is the diagonal eigenvalue matrix of

$$\mathbf{M} = \boldsymbol{\Delta}^2 + 2\mathbf{V} \tag{81}$$

with

$$\mathbf{V} = \boldsymbol{\Delta}^{1/2}\mathbf{B}\mathbf{B}^{\mathrm{T}}\boldsymbol{\Delta}^{1/2} \tag{82}$$

and $\mathbf{U}^{(0)}$ diagonalizes the zero-order eigenvalue problem,

$$((\mathbf{U}^{(0)})^{-1}\boldsymbol{\Delta}^2\mathbf{U}^{(0)})_{ia\sigma jb\sigma'} = \delta_{\sigma\sigma'}\delta_{ij}\delta_{ab}(\varepsilon_{a\sigma} - \varepsilon_{i\sigma}) \tag{83}$$

To obtain E^{d} and $E^{\mathrm{d}}_{\mathrm{g}}$ from eq 80, $\boldsymbol{\Omega}^2$ was replaced by the diagonal matrix of its first-order approximation

$$\tilde{\Omega}^2_{ia\sigma jb\sigma'} = \delta_{\sigma\sigma'}\delta_{ij}\delta_{ab}((\mathbf{U}^{(0)})^{-1}\mathbf{M}\mathbf{U}^{(0)})_{ia\sigma ia\sigma} \tag{84}$$

dx.doi.org/10.1021/ct4008553 | J. Chem. Theory Comput. 2014, 10, 180−194

for a perturbation 2**V**. Using canonical KS MOs, $\boldsymbol{\Delta}^2$ is diagonal and thus $\mathbf{U}^{(0)} = \mathbf{1}$. This yields [cf. ref 45]

$$\tilde{\Omega}^2_{ia\sigma jb\sigma'} = \delta_{\sigma\sigma'}\delta_{ij}\delta_{ab}M_{ia\sigma ia\sigma} \tag{85}$$

Expression 84 is used to form derivatives and canonical MOs are subsequently assumed. Further, the frequency integral in eq 80 is replaced for E_g^d by a finite summation over grid points, while E^d is obtained by analytical evaluation. The result for E^d was given in equation 36 of ref 45.

The derivatives of L_g^{RIRPA} with respect to the Lagrange multipliers $\mathcal{T}$, $\mathcal{D}^\Delta$, and $\mathcal{W}$ form the constraints 78, 22, and 23. Together with the stationarity conditions 24 and 25, where L_g^{RIRPA} must be used, and

$$\left(\frac{\partial L_g^{\mathrm{RIRPA}}}{\partial \mathcal{A}}\right)_{\mathrm{stat}} = 0 \tag{86}$$

the stationary point of L_g^{RIRPA} is determined as "stat = ($\boldsymbol{C} = \mathbf{C}$, $\boldsymbol{\mathcal{E}} = \boldsymbol{\varepsilon}$, $\mathcal{A} = a$, $\mathcal{T} = \tau$, $\boldsymbol{\mathcal{D}}^\Delta = \mathbf{D}^\Delta$, $\boldsymbol{\mathcal{W}} = \mathbf{W}$)". At the stationary point, we obtain

$$E_g^{\mathrm{RIRPA}}(\mathbf{C}, \boldsymbol{\varepsilon}, a|\mathbf{X}) = L_g^{\mathrm{RIRPA}}(\boldsymbol{C}, \boldsymbol{\mathcal{E}}, \mathcal{A}, \mathcal{T}, \boldsymbol{\mathcal{D}}^\Delta, \boldsymbol{\mathcal{W}}|\mathbf{X}, \mathbf{V}^{\mathrm{XC}}, \mathbf{S})|_{\mathrm{stat}} \tag{87}$$

which replaces eq 26. From eq 87, the derivative equation is derived which is analogous to eq 27 but uses the grid dependent functionals E_g^{RIRPA} and L_g^{RIRPA}. From this equation, it follows that the total derivative $\mathrm{d}E_g^{\mathrm{RIRPA}}/\mathrm{d}\xi$ may be calculated as given in eq 42; however, the grid-corrected quantities must be used, as explained below.

The Lagrange multiplier

$$\tau = \left(\frac{\partial E_g^{\mathrm{C\,RIRPA}}/\partial\mathcal{A}}{\partial E_g^{\mathrm{d}}/\partial\mathcal{A}}\right)_{\mathrm{stat}} \tag{88}$$

is obtained by expansion of the derivative in eq 86 using eq 77 together with the derivatives

$$\left(\frac{\partial E_g^{\mathrm{C\,RIRPA}}}{\partial\mathcal{A}}\right)_{\mathrm{stat}} = \frac{1}{a}\left(E_g^{\mathrm{C\,RIRPA}} - 2\sum_{\alpha=1}^{N_g}\frac{w_\alpha}{2\pi}\omega_\alpha^2 \times \langle\tilde{\mathbf{Q}}(\omega_\alpha)\mathbf{B}^T\mathbf{d}^{-1}(\omega_\alpha)\boldsymbol{\Delta}\mathbf{d}^{-1}(\omega_\alpha)\mathbf{B}\rangle\right) \tag{89}$$

and

$$\left(\frac{\partial E_g^{\mathrm{d}}}{\partial\mathcal{A}}\right)_{\mathrm{stat}} = \frac{1}{a}\left(E_g^{\mathrm{d}} - 2\sum_{\alpha=1}^{N_g}\frac{w_\alpha}{2\pi}\omega_\alpha^2\langle\mathbf{B}^{\mathrm{T}}\mathbf{g}(\omega_\alpha)\mathbf{B}\rangle\right) \tag{90}$$

where

$$\mathbf{g}(\omega) = \mathbf{G}(\omega)(\mathbf{m}^{-1}(\omega) - \mathbf{d}^{-1}(\omega)) \tag{91}$$

$$\mathbf{m}(\omega) = \omega^2\mathbf{1} + \tilde{\boldsymbol{\Omega}}^2 \tag{92}$$

$$\mathbf{d}(\omega) = \omega^2\mathbf{1} + \boldsymbol{\Delta}^2 \tag{93}$$

Next, $\mathbf{D}^\Delta$ and $\mathbf{W}$ are determined from the stationarity eqs 24 and 25, which contain contributions from E^d and E_g^d and lead to eq 28 with matrix $\mathbf{T}$ given by

$$\mathbf{T} = \mathbf{T}_g + \tau\mathbf{T}^\Delta \tag{94}$$

where $\mathbf{T}_g$ is defined with eqs 29 and 30 replacing integrals by finite sums over the frequency grid. $\mathbf{T}^\Delta$ is defined as

$$\mathbf{T}^\Delta = \left(\frac{\partial E^{\mathrm{d}}}{\partial\boldsymbol{\mathcal{E}}}\right)_{\mathrm{stat}} - \left(\frac{\partial E_g^{\mathrm{d}}}{\partial\boldsymbol{\mathcal{E}}}\right)_{\mathrm{stat}} \tag{95}$$

The partial derivatives of the approximate energies are

$$\left(\frac{\partial E_{(g)}^{\mathrm{d}}}{\partial\mathcal{E}_{ij\sigma}}\right)_{\mathrm{stat}} = \frac{1}{2}\sum_a A^{\mathrm{d}}_{(g)ia\sigma ja\sigma} \quad \text{and}$$
$$\left(\frac{\partial E_{(g)}^{\mathrm{d}}}{\partial\mathcal{E}_{ab\sigma}}\right)_{\mathrm{stat}} = -\frac{1}{2}\sum_i A^{\mathrm{d}}_{(g)ia\sigma ib\sigma} \tag{96}$$

where the subscript "(g)" means that the equation is valid for both, analytical and numerical integration. The matrix $\mathbf{A}^{\mathrm{d}}_{(g)}$ is

$$A^{\mathrm{d}}_{(g)ia\sigma jb\sigma} = \frac{A^{(1)\mathrm{d}}_{(g)jb\sigma ia\sigma}}{\Delta_{ia\sigma} - \Delta_{jb\sigma}} - A^{(2)\mathrm{d}}_{(g)ia\sigma jb\sigma} - \frac{A^{(3)\mathrm{d}}_{(g)ia\sigma jb\sigma}}{\sqrt{\Delta_{ia\sigma}} + \sqrt{\Delta_{ja\sigma}}} \tag{97}$$

where the $\mathbf{A}^{(1)\mathrm{d}}_{(g)}$ contribution vanishes for $ia = jb$. Further, the three contributions to the $\mathbf{A}^{\mathrm{d}}$ matrix are

$$\mathbf{A}^{(1)\mathrm{d}}_\sigma = \frac{1}{2}(\mathbf{M}_{\mathrm{sqd},\sigma}\mathbf{M}_\sigma - \mathbf{M}_\sigma\mathbf{M}_{\mathrm{sqd},\sigma}) \tag{98}$$

$$\mathbf{A}^{(2)\mathrm{d}}_\sigma = \frac{1}{2}\boldsymbol{\Delta}_\sigma\mathbf{M}_{\mathrm{sqd},\sigma} + \frac{1}{2}\mathbf{M}_{\mathrm{sqd},\sigma}\boldsymbol{\Delta}_\sigma - \mathbf{1} \tag{99}$$

$$\mathbf{A}^{(3)\mathrm{d}}_\sigma = \mathbf{B}_\sigma\mathbf{B}^{\mathrm{T}}_\sigma\boldsymbol{\Delta}^{1/2}_\sigma\mathbf{M}_{\mathrm{sqd},\sigma} + \mathbf{M}_{\mathrm{sqd},\sigma}\boldsymbol{\Delta}^{1/2}_\sigma\mathbf{B}_\sigma\mathbf{B}^{\mathrm{T}}_\sigma \tag{100}$$

with

$$\mathbf{M}_{\mathrm{sqd}} = \tilde{\boldsymbol{\Omega}}^{-1} \tag{101}$$

For the terms evaluated on the grid, the $\mathbf{A}^{\mathrm{d}}_g$ matrix contains

$$\mathbf{A}^{(1)\mathrm{d}}_{g\sigma} = \sum_{\alpha=1}^{N_g}\frac{w_\alpha}{2\pi}([\mathbf{g}_\sigma\boldsymbol{\Delta}^2_\sigma + 2\mathbf{m}^{-1}_\sigma\mathbf{V}_\sigma] - [\boldsymbol{\Delta}^2_\sigma\mathbf{g}_\sigma + 2\mathbf{V}_\sigma\mathbf{m}^{-1}_\sigma]) \tag{102}$$

$$\mathbf{A}^{(2)\mathrm{d}}_{g\sigma} = \sum_{\alpha=1}^{N_g}\frac{w_\alpha}{2\pi}(\boldsymbol{\Delta}_\sigma[\mathbf{g}_\sigma + 2\mathbf{d}^{-1}_\sigma\mathbf{V}_\sigma\mathbf{d}^{-1}_\sigma] + [\mathbf{g}_\sigma + 2\mathbf{d}^{-1}_\sigma\mathbf{V}_\sigma\mathbf{d}^{-1}_\sigma]\boldsymbol{\Delta}_\sigma) \tag{103}$$

$$\mathbf{A}^{(3)\mathrm{d}}_{g\sigma} = 2\sum_{\alpha=1}^{N_g}\frac{w_\alpha}{2\pi}(\mathbf{B}_\sigma\mathbf{B}^{\mathrm{T}}_\sigma\boldsymbol{\Delta}^{1/2}_\sigma\mathbf{g}_\sigma + \mathbf{g}_\sigma\boldsymbol{\Delta}^{1/2}_\sigma\mathbf{B}_\sigma\mathbf{B}^{\mathrm{T}}_\sigma) \tag{104}$$

$\mathbf{Z}$ in eq 28 is the solution of a single CPKS equation, where $\mathbf{T}$ of eq 94 and

$$\boldsymbol{\gamma} = \boldsymbol{\gamma}_g + \tau\boldsymbol{\gamma}^\Delta \tag{105}$$

are used in the right hand side $\mathbf{R}$ given by eq 36. $\boldsymbol{\gamma}_g$ is defined with eqs 39 and 40 replacing integrals by finite sums. The correction term

dx.doi.org/10.1021/ct4008553 | J. Chem. Theory Comput. 2014, 10, 180−194

$$\gamma^{\Delta}_{pq\sigma} = \sum_{\mu} \left(\frac{\partial (E^{\mathrm{d}} - E^{\mathrm{d}}_{\mathrm{g}})}{\partial C_{\mu p\sigma}} \right)_{\mathrm{stat}} C_{\mu q\sigma} \tag{106}$$

requires orbital derivatives of approximate correlation energies,

$$\sum_{\mu} \left(\frac{\partial E^{\mathrm{d}}_{(\mathrm{g})}}{\partial C_{\mu a\sigma}} \right)_{\mathrm{stat}} C_{\mu q\sigma} = \sum_{i} (\mathbf{G}^{\mathrm{d}}_{(\mathrm{g})}\mathbf{B}\mathbf{B}^{\mathrm{T}})_{ia\sigma iq\sigma} \tag{107}$$

$$\sum_{\mu} \left(\frac{\partial E^{\mathrm{d}}_{(\mathrm{g})}}{\partial C_{\mu i\sigma}} \right)_{\mathrm{stat}} C_{\mu q\sigma} = \sum_{a} (\mathbf{G}^{\mathrm{d}}_{(\mathrm{g})}\mathbf{B}\mathbf{B}^{\mathrm{T}})_{ia\sigma qa\sigma} \tag{108}$$

where $\mathbf{G}^{\mathrm{d}}$ and $\mathbf{G}^{\mathrm{d}}_{\mathrm{g}}$ are defined by

$$\mathbf{G}^{\mathrm{d}} = \mathbf{\Delta}^{1/2}\mathbf{M}_{\mathrm{sqd}}\mathbf{\Delta}^{1/2} - \mathbf{1} \tag{109}$$

$$\mathbf{G}^{\mathrm{d}}_{\mathrm{g}} = 2\sum_{\alpha=1}^{N_g} \frac{w_\alpha}{2\pi} \mathbf{\Delta}^{1/2}\mathbf{g}\mathbf{\Delta}^{1/2} \tag{110}$$

$\mathbf{D}^{\Delta} = \mathbf{T} + \mathbf{Z}$ and $\boldsymbol{\gamma}$ from eqs 94, 105, and the subsequently solved CPKS equation may be used to evaluate the energy-weighted density matrix $\mathbf{W}$, eqs 41. All of these grid-corrected quantities go finally into the energy gradients, eq 42. $\mathbf{\Gamma}^{(4)}$ is indirectly corrected through $\mathbf{D}^{\Delta}$, whereas $\mathbf{\Gamma}^{(3)}$ and $\mathbf{\Gamma}^{(2)}$ contain direct correction terms,

$$\Gamma^{(3)}_{P\mu\nu\sigma} = \Gamma^{(3)}_{\mathrm{g},P\mu\nu\sigma} + \tau \sum_{ia} C_{\mu i\sigma}C_{\nu a\sigma}[(\mathbf{G}^{\mathrm{d}} - \mathbf{G}^{\mathrm{d}}_{\mathrm{g}})\mathbf{B}(\mathbf{\Lambda}^{-1})^{\mathrm{T}}]_{ia\sigma P} \tag{111}$$

$$\Gamma^{(2)}_{QP} = \Gamma^{(2)}_{\mathrm{g},QP} - \tau[\mathbf{\Lambda}^{-1}\mathbf{B}^{\mathrm{T}}(\mathbf{G}^{\mathrm{d}} - \mathbf{G}^{\mathrm{d}}_{\mathrm{g}})\mathbf{B}(\mathbf{\Lambda}^{-1})^{\mathrm{T}}]_{PQ} \tag{112}$$

where $\mathbf{\Gamma}^{(3)}_{\mathrm{g}}$ and $\mathbf{\Gamma}^{(2)}_{\mathrm{g}}$ are defined with eqs 51 and 52 replacing integrals by finite sums. In the limit of large grids ($N_g \to \infty$), the corrections in $\mathbf{T}$, $\boldsymbol{\gamma}$, $\mathbf{\Gamma}^{(3)}$, and $\mathbf{\Gamma}^{(2)}$ due to the perturbed grid vanish and the "g" indexed terms become equivalent to the corresponding analytical integrals.

■ ASSOCIATED CONTENT

Supporting Information

Full details on the definition of the sensitivity measure and selecting its thresholds for numerically accurate RI-RPA energies and gradients. Definitions of intermonomer distances for the dimers in the A24 test set. Coordinates for the RI-RPA-optimized transition metal complexes and the dimers. This material is available free of charge via the Internet at http://pubs.acs.org.

■ AUTHOR INFORMATION

Corresponding Authors

*E-mail: filipp.furche@uci.edu.

Notes

The authors declare the following competing financial interest(s): Filipp Furche has an equity interest in Turbomole GmbH, a company that may potentially benefit from the research results, and also serves as a Scientific Coordinator for the company. The terms of this arrangement have been reviewed and approved by the University of California, Irvine, in accordance with its conflict of interest policies.

■ ACKNOWLEDGMENTS

Asbjörn M. Burow thanks the Deutsche Forschungsgemeinschaft (DFG Research Fellowship BU 2874/1-1) for a postdoctoral scholarship. This material is based upon work supported by the National Science Foundation under CHE-0911266 and CHE-1213382.

■ REFERENCES

(1) Crabtree, R. H. *The Organometallic Chemistry of the Transition Metals*; Wiley: Hoboken, NJ, 2009.
(2) Ziegler, T. A Chronicle About the Development of Electronic Structure Theories for Transition Metal Complexes. In *Molecular Electronic Structures of Transition Metal Complexes II*; Mingos, D. M. P., Day, P., Dahl, J. P., Eds.; Structure and Bonding; Springer: Berlin, 2012; Vol. *143*; pp 1−38.
(3) Wang, Y.-T.; Jin, K. J.; Leopold, S. H.; Wang, J.; Peng, H.-L.; Platz, M. S.; Xue, J.; Phillips, D. L.; Glover, S. A.; Novak, M. *J. Am. Chem. Soc.* **2008**, *130*, 16021−16030.
(4) Asmis, K. R. *Phys. Chem. Chem. Phys.* **2012**, *14*, 9270−9281.
(5) Savoca, M.; Langer, J.; Harding, D. J.; Dopfer, O.; Fielicke, A. *Chem. Phys. Lett.* **2013**, *557*, 49−52.
(6) Parr, R. G.; Yang, W. *Density-Functional Theory of Atoms and Molecules*; Oxford University Press, 1989.
(7) Becke, A. D. *J. Chem. Phys.* **1993**, *98*, 5648−5652.
(8) Lee, C.; Yang, W.; Parr, R. G. *Phys. Rev. B* **1988**, *37*, 785−789.
(9) Perdew, J. P.; Burke, K.; Ernzerhof, M. *Phys. Rev. Lett.* **1996**, *77*, 3865−3868.
(10) Hay, P. J.; Martin, R. L.; Uddin, J.; Scuseria, G. E. *J. Chem. Phys.* **2006**, *125*, 034712.
(11) Sieffert, N.; Bühl, M. *Inorg. Chem.* **2009**, *48*, 4622−4624.
(12) Siegbahn, P. E. M.; Blomberg, M. R. A.; Chen, S.-L. *J. Chem. Theory Comput.* **2010**, *6*, 2040−2044.
(13) Jacobsen, H.; Cavallo, L. *ChemPhysChem* **2012**, *13*, 562−569.
(14) Minenkov, Y.; Singstad, Å.; Occhipinti, G.; Jensen, V. R. *Dalton Trans.* **2012**, *41*, 5526−5541.
(15) Sanford, M. S.; Love, J. A.; Grubbs, R. H. *J. Am. Chem. Soc.* **2001**, *123*, 6543−6554.
(16) Eshuis, H.; Furche, F. *J. Chem. Phys.* **2012**, *136*, 084105.
(17) Grimme, S.; Antony, J.; Ehrlich, S.; Krieg, H. *J. Chem. Phys.* **2010**, *132*, 154104.
(18) Zhao, Y.; Truhlar, D. G. *Acc. Chem. Res.* **2008**, *41*, 157−167.
(19) Zhao, Y.; Truhlar, D. G. *Chem. Phys. Lett.* **2011**, *502*, 1−13.
(20) Møller, C.; Plesset, M. S. *Phys. Rev.* **1934**, *46*, 618−622.
(21) Raghavachari, K.; Trucks, G. W.; Pople, J. A.; Head-Gordon, M. *Chem. Phys. Lett.* **1989**, *157*, 479−483.
(22) Shavitt, I.; Bartlett, R. J. *Many-Body Methods in Chemistry and Physics: MBPT and Coupled-Cluster Theory*; Cambridge University Press: Cambridge, 2009.
(23) Roos, B. O.; Linse, P.; Siegbahn, P. E. M.; Blomberg, M. R. A. *Chem. Phys.* **1982**, *66*, 197−207.
(24) Andersson, K.; Malmqvist, P.-Å.; Roos, B. O. *J. Chem. Phys.* **1992**, *96*, 1218−1226.
(25) Buenker, R. J.; Peyerimhoff, S. D. *Theor. Chim. Acta* **1974**, *35*, 33−58.
(26) Bruna, P. J.; Dohmann, H.; Peyerimhoff, S. D. *Can. J. Phys.* **1984**, *62*, 1508−1523.
(27) Furche, F. *Phys. Rev. B* **2001**, *64*, 195120.
(28) Fuchs, M.; Gonze, X. *Phys. Rev. B* **2002**, *65*, 235109.
(29) Hellgren, M.; von Barth, U. *Phys. Rev. B* **2007**, *76*, 075107.
(30) Jiang, H.; Engel, E. *J. Chem. Phys.* **2007**, *127*, 184108.
(31) Heßelmann, A.; Görling, A. *Mol. Phys.* **2011**, *109*, 2473−2500.
(32) Eshuis, H.; Bates, J. E.; Furche, F. *Theor. Chem. Acc.* **2012**, *131*, 1084.
(33) Nekovee, M.; Pitarke, J. *Comput. Phys. Commun.* **2001**, *137*, 123−142.
(34) Ren, X.; Rinke, P.; Scheffler, M. *Phys. Rev. B* **2009**, *80*, 045402.
(35) Harl, J.; Kresse, G. *Phys. Rev. B* **2008**, *77*, 045136.

(36) Grüneis, A.; Marsman, M.; Harl, J.; Schimka, L.; Kresse, G. *J. Chem. Phys.* **2009**, *131*, 154115.
(37) Harl, J.; Schimka, L.; Kresse, G. *Phys. Rev. B* **2010**, *81*, 115126.
(38) Björkman, T.; Gulans, A.; Krasheninnikov, A. V.; Nieminen, R. M. *Phys. Rev. Lett.* **2012**, *108*, 235502.
(39) Paier, J.; Ren, X.; Rinke, P.; Scuseria, G. E.; Grüneis, A.; Kresse, G.; Scheffler, M. *New J. Phys.* **2012**, *14*, 043002.
(40) Del Ben, M.; Hutter, J.; VandeVondele, J. *J. Chem. Theory Comput.* **2013**, *9*, 2654−2671.
(41) Gould, T.; Dobson, J. F.; Lebègue, S. *Phys. Rev. B* **2013**, *87*, 165422.
(42) Eshuis, H.; Furche, F. *J. Phys. Chem. Lett.* **2011**, *2*, 983−989.
(43) Rekkedal, J.; Coriani, S.; Iozzi, M. F.; Teale, A. M.; Helgaker, T.; Pedersen, T. B. *J. Chem. Phys.* **2013**, *139*, 081101.
(44) Scuseria, G. E.; Henderson, T. M.; Sorensen, D. C. *J. Chem. Phys.* **2008**, *129*, 231101.
(45) Eshuis, H.; Yarkony, J.; Furche, F. *J. Chem. Phys.* **2010**, *132*, 234114.
(46) Neumann, R.; Nobes, R. H.; Handy, N. C. *Mol. Phys.* **1996**, *87*, 1−36.
(47) Pople, J. A.; Gill, P. M. W.; Johnson, B. G. *Chem. Phys. Lett.* **1992**, *199*, 557−560.
(48) Helgaker, T.; Jørgensen, P.; Handy, N. C. *Theor. Chim. Acta* **1989**, *76*, 227−245.
(49) Pulay, P.; Saebø, S. *Theor. Chim. Acta* **1986**, *69*, 357−368.
(50) Baerends, E. J.; Ellis, D. E.; Ros, P. *Chem. Phys.* **1973**, *2*, 41−51.
(51) Dunlap, B. I.; Connolly, J. W. D.; Sabin, J. R. *J. Chem. Phys.* **1979**, *71*, 3396−3402.
(52) Boyd, J. P. *J. Sci. Comput.* **1987**, *2*, 99−109.
(53) Furche, F. *J. Chem. Phys.* **2001**, *114*, 5982−5992.
(54) Ren, X.; Rinke, P.; Blum, V.; Wieferink, J.; Tkatchenko, A.; Sanfilippo, A.; Reuter, K.; Scheffler, M. *New J. Phys.* **2012**, *14*, 053020.
(55) Jørgensen, P.; Simons, J. *Geometrical Derivatives of Energy Surfaces and Molecular Properties*; Nato Science Series C; D. Reidel Publishing Co.: Dordrecht, The Netherlands, 1986; Vol. *166*.
(56) Head-Gordon, M.; Pople, J. A. *J. Chem. Phys.* **1988**, *89*, 5777−5786.
(57) Helgaker, T.; Taylor, P. R. *Theor. Chim. Acta* **1992**, *83*, 177−183.
(58) Sternheimer, R. M. *Phys. Rev.* **1954**, *96*, 951−968.
(59) Dalgarno, A.; Stewart, A. L. *Proc. R. Soc. Lond. A* **1958**, *247*, 245−259.
(60) Helgaker, T.; Jørgensen, P. *Theor. Chim. Acta* **1989**, *75*, 111−127.
(61) Furche, F.; Ahlrichs, R. *J. Chem. Phys.* **2002**, *117*, 7433−7447.
(62) Ullrich, C. A. *Time-Dependent Density-Functional Theory—Concepts and Applications*; Oxford University Press: Oxford, 2012.
(63) McWeeny, R. *Proc. R. Soc. Lond. A* **1956**, *235*, 496−509.
(64) Furche, F.; Rappoport, D. Density Functional Methods for Excited States: Equilibrium Structure and Electronic Spectra. In *Computational Photochemistry*; Olivucci, M., Ed.; Theoretical and Computational Chemistry; Elsevier: Amsterdam, 2005; Vol. *16*; pp 93−128.
(65) Deglmann, P.; Furche, F.; Ahlrichs, R. *Chem. Phys. Lett.* **2002**, *362*, 511−518.
(66) Weigend, F.; Ahlrichs, R. *Phys. Chem. Chem. Phys.* **2005**, *7*, 3297−3305.
(67) Weigend, F.; Häser, M. *Theor. Chem. Acc.* **1997**, *97*, 331−340.
(68) Jung, Y.; Lochan, R. C.; Dutoi, A. D.; Head-Gordon, M. *J. Chem. Phys.* **2004**, *121*, 9793−9802.
(69) Almlöf, J. *Chem. Phys. Lett.* **1991**, *181*, 319−320.
(70) Häser, M.; Almlöf, J. *J. Chem. Phys.* **1992**, *96*, 489−494.
(71) Ayala, P. Y.; Kudin, K. N.; Scuseria, G. E. *J. Chem. Phys.* **2001**, *115*, 9698−9707.
(72) Häser, M. *Theor. Chim. Acta* **1993**, *87*, 147−173.
(73) Schweizer, S.; Doser, B.; Ochsenfeld, C. *J. Chem. Phys.* **2008**, *128*, 154101.
(74) Maurer, S. A.; Lambrecht, D. S.; Kussmann, J.; Ochsenfeld, C. *J. Chem. Phys.* **2013**, *138*, 014101.
(75) *TURBOMOLE* version 6.5; Turbomole GmbH: Karlsruhe, 2013; available from http://www.turbomole.com.
(76) Ahlrichs, R.; Bär, M.; Häser, M.; Horn, H.; Kölmel, C. *Chem. Phys. Lett.* **1989**, *162*, 165−169.
(77) Adamo, C.; Barone, V. *J. Chem. Phys.* **1999**, *110*, 6158−6170.
(78) Treutler, O.; Ahlrichs, R. *J. Chem. Phys.* **1995**, *102*, 346−354.
(79) Weigend, F. *Phys. Chem. Chem. Phys.* **2006**, *8*, 1057−1065.
(80) Weigend, F.; Köhn, A.; Hättig, C. *J. Chem. Phys.* **2002**, *116*, 3175−3183.
(81) Hättig, C. *Phys. Chem. Chem. Phys.* **2005**, *7*, 59−66.
(82) Weigend, F. *Phys. Chem. Chem. Phys.* **2002**, *4*, 4285−4291.
(83) Dunning, T. H., Jr. *J. Chem. Phys.* **1989**, *90*, 1007−1023.
(84) Woon, D. E.; Dunning, T. H., Jr. *J. Chem. Phys.* **1993**, *98*, 1358−1371.
(85) Balabanov, N. B.; Peterson, K. A. *J. Chem. Phys.* **2005**, *123*, 064107.
(86) Rappoport, D.; Furche, F. *J. Chem. Phys.* **2010**, *133*, 134105.
(87) Eichkorn, K.; Treutler, O.; Öhm, H.; Häser, M.; Ahlrichs, R. *Chem. Phys. Lett.* **1995**, *240*, 283−290.
(88) Hättig, C. *J. Chem. Phys.* **2003**, *118*, 7751−7761.
(89) Pawłowski, F.; Jørgensen, P.; Olsen, J.; Hegelund, F.; Helgaker, T.; Gauss, J.; Bak, K. L.; Stanton, J. F. *J. Chem. Phys.* **2002**, *116*, 6482−6496.
(90) Cook, R. L. *J. Mol. Struct.* **1975**, *28*, 237−246.
(91) Bühl, M.; Kabrede, H. *J. Chem. Theory Comput.* **2006**, *2*, 1282−1290.
(92) Klopper, W.; Lüthi, H. P. *Chem. Phys. Lett.* **1996**, *262*, 546−552.
(93) Hu, Z.; Boyd, R. J. *J. Chem. Phys.* **2000**, *113*, 9393−9401.
(94) Ehlers, A. W.; Frenking, G. *J. Am. Chem. Soc.* **1994**, *116*, 1514−1520.
(95) Hrušák, J.; Hertwig, R. H.; Schröder, D.; Schwerdtfeger, P.; Koch, W.; Schwarz, H. *Organometallics* **1995**, *14*, 1284−1291.
(96) Beagley, B.; Schmidling, D. *J. Mol. Struct.* **1974**, *22*, 466−468.
(97) Hedberg, L.; Iijima, T.; Hedberg, K. *J. Chem. Phys.* **1979**, *70*, 3224−3229.
(98) Řezáč, J.; Hobza, P. *J. Chem. Theory Comput.* **2013**, *9*, 2151−2155.
(99) Kristyán, S.; Pulay, P. *Chem. Phys. Lett.* **1994**, *229*, 175−180.
(100) Grimme, S. *J. Comput. Chem.* **2006**, *27*, 1787−1799.
(101) Toulouse, J.; Zhu, W.; Ángyán, J. G.; Savin, A. *Phys. Rev. A* **2010**, *82*, 032502.
(102) Rauhut, G.; Pulay, P. *J. Phys. Chem.* **1995**, *99*, 3093−3100.
(103) Merrick, J. P.; Moran, D.; Radom, L. *J. Phys. Chem. A* **2007**, *111*, 11683−11700.
(104) Heßelmann, A.; Görling, A. *Mol. Phys.* **2010**, *108*, 359−372.
(105) Hellgren, M.; von Barth, U. *J. Chem. Phys.* **2010**, *132*, 044101.
(106) Hellgren, M.; Rohr, D. R.; Gross, E. K. U. *J. Chem. Phys.* **2012**, *136*, 034106.
(107) Bleiziffer, P.; Heßelmann, A.; Görling, A. *J. Chem. Phys.* **2013**, *139*, 084113.
(108) McClelland, B. W.; Robiette, A. G.; Hedberg, L.; Hedberg, K. *Inorg. Chem.* **2001**, *40*, 1358−1362.
(109) Haaland, A.; Vilkov, L.; Khaikin, L. S.; Yokozeki, A.; Bauer, S. H. *Top. Curr. Chem.* **1975**, *53*, 1−23.
(110) Adamo, C.; Cossi, M.; Scalmani, G.; Barone, V. *Chem. Phys. Lett.* **1999**, *307*, 265−271.
(111) Sekino, H.; Bartlett, R. J. *J. Chem. Phys.* **1993**, *98*, 3022−3037.
(112) Huber, K. P.; Herzberg, G. *Molecular Spectra and Molecular Structure. IV. Constants of Diatomic Molecules*; Van Nostrand Reinhold: New York, 1979.
(113) Oh, J. J.; Hillig, K. W.; Kuczkowski, R. L.; Bohn, R. K. *J. Phys. Chem.* **1990**, *94*, 4453−4455.
(114) Lovas, F. J.; Suenram, R. D.; Coudert, L. H.; Blake, T. A.; Grant, K. J.; Novick, S. E. *J. Chem. Phys.* **1990**, *92*, 891−898.
(115) Dyke, T. R.; Mack, K. M.; Muenter, J. S. *J. Chem. Phys.* **1977**, *66*, 498−510.
(116) Canagaratna, M.; Ott, M. E.; Leopold, K. R. *Chem. Phys. Lett.* **1997**, *281*, 63−68.

(117) Ruden, T. A.; Helgaker, T.; Jørgensen, P.; Olsen, J. *J. Chem. Phys.* **2004**, *121*, 5874−5884.
(118) Hoy, A. R.; Mills, I. M.; Strey, G. *Mol. Phys.* **1972**, *24*, 1265−1290.
(119) Allen, H. C.; Plyler, E. K. *J. Chem. Phys.* **1956**, *25*, 1132−1136.
(120) Sauer, J.; Döbler, J. *ChemPhysChem* **2005**, *6*, 1706−1710.
(121) Martin, J. M. L.; Lee, T. J.; Taylor, P. R. *J. Chem. Phys.* **1992**, *97*, 8361−8371.
(122) Uhlár, M.; Pitoňák, M.; Černušák, I. *Mol. Phys.* **2005**, *103*, 2309−2319.
(123) Pawłowski, F.; Halkier, A.; Jørgensen, P.; Bak, K. L.; Helgaker, T.; Klopper, W. *J. Chem. Phys.* **2003**, *118*, 2539−2549.